5-2013

Modal Analysis to Minimize Gearbox Induced Noise of General Electric Wind Turbines

Matthew Evans
Clemson University, matt.r.evans7@gmail.com

MODAL ANALYSIS TO MINIMIZE GEARBOX INDUCED NOISE OF GENERAL ELECTRIC WIND TURBINES

A Thesis
Presented to
the Graduate School of
Clemson University

In Partial Fulfillment
of the Requirements for the Degree
Master of Science
Mechanical Engineering

by
Matthew Richard Evans
May 2013

Accepted by:
Dr. Mohammed F. Daqaq, Committee Chair
Dr. Lonny Thompson
Dr. Gang Li

ABSTRACT

With the current global emphasis on alternative green energy sources, wind turbine technologies have seen significant growth in recent years. Today, wind turbines are being produced and constructed at unprecedented levels with their sites inching closer and closer to residential communities. With that, wind turbine companies have been receiving growing complains about the noise emitted from these turbines during operation. To resolve this issue, many of these companies are spending more resources to design and manufacture quieter wind turbines. In particular, General Electric (GE) intends to reduce the noise created by their 2.5 MW CGDT wind turbines. Previous studies showed that noise starts in the gearbox due to the transmission error between the meshing gears which creates extensive vibrations. These vibrations resonate with the gearbox housing causing energy to propagate from the housing to the bedplate and then to the nacelle. Vibrations are then transmitted from the nacelle to the rotating blades which produce a humming sound (noise) in the surroundings.

GE researchers have theorized that noise can be eliminated if the gearbox housing is designed such that its modal frequencies are far from the excitation frequencies resulting from the transmission error. In order to achieve this goal, this Thesis aims to develop a computational model which captures the modal response of the gearbox housing. Once this model is developed and validated against experimental

data, alterations to the design can be implemented to shift the trouble frequencies. Two computational models are developed using the commercial softwares ANSYS and MASTA. The ANSYS model, which imposes several simplifying assumptions on the dynamics, is shown to lack the accuracy necessary to capture the modal response of the gearbox housing. The MASTA model, on the other hand, includes the interactions between the gearbox dynamics and the housing and is shown to produce modal responses that match the experimental data. The model and techniques provided in this Thesis will provide the springboard upon which future design improvements and noise reduction techniques of GE wind turbines are launched.

DEDICATION

To my heavenly Father and His son Jesus Christ for being my ever present Rock and

Fortress, my continual Comforter and Guide, my everlasting God and Savior

ACKNOWLEDGMENTS

I immensely thank my family. My parents, Spencer and Lora Evans, for their constant love, encouragement, and support. They instilled in me from a young age the value of hard work and persistence. Those two characteristics have been necessary for me to reach this point. My siblings Daniel, Rebekah, and Caleb for their love and friendship.

My loving wife Davis has been with me through it all and has supported and encouraged me along the way, and for that I want to thank her. She has been there by my side through the many long nights. She has seen me during times of high stress and been patient and loving towards me throughout. It has been a long road for us. God has been doing exciting things in our lives and we are truly grateful for His blessings.

Finally, I want to thank my God and Savior Jesus Christ for His many blessings. It is only because of Him that I have anything and it is only through Him that I can do anything. He is the One who has had His precious, sovereign hand over all of my life and who has brought me to this point. I look forward to seeing with this graduate degree where God will lead my wife and I and who He will place around us. I pray that I will never be prideful because of this degree but instead that God would use this degree as a tool to allow me to reach people that I otherwise would not have been able to reach.

Table of Contents

Table of Contents (Continued)

Table of Contents (Continued)

LIST OF FIGURES

List of Figures (Conitnued)

List of Figures (Continued)

Figure   Page

LIST OF TABLES

CHAPTER 1: INTRODUCTION

1.1: Motivation

The modern world depends very heavily on electricity. Combustible fuels, which include gas and coal, produce the majority of the electricity in the United States (US). To reduce the US dependency on foreign countries for these resources, great steps have been taken to develop alternative sources of energy. To encourage and aid in this development, many nations, not just the US, are now providing financial support and incentives to companies and individuals who participate in this so called "green initiative". Alternative sources of energy that are leading the way in this "green initiative" are solar and wind power. As a result of this new initiative the wind turbine industry has seen significant growth since the early 21st century.

Wind turbines have several complaints against them from reducing property value, to scenery destruction, to blade flicker, to noise. The biggest of these complaints is the noise that they produce. For that reason, it is in this area that a lot of research and improvement has been made in the last five years. Despite the improvements, noise remains one of the largest problems for wind turbine commercialization. General Electric (GE) wants to reduce the amount of noise that their wind turbines produce. The

motivation behind this is to increase public appeal which will help them remain one of the leading wind turbine manufacturers in the world.

1.2: Wind Turbine Overview

Harnessing wind to perform work is something mankind has been doing for a long time. The modern day wind turbine performs the same basic task as a wind mill. Although the output is different, the principle concept is the same: harness wind energy and transform it to perform a desired function. While there is some controversy as to how long wind mills have been used, most agree that it was the Persians who first started using them [1, 2]. There is some evidence that the Persians were using them as early as 200 B.C. [1]. Wind mills have been used throughout ancient times as a way of obtaining free power to grind grain and transport water [1, 2, 3]. They were used extensively in the Persian Empire during the 9th century [4]. In the early 12th century of England and France, wind mills became more prevalent as a way for people to become independent of the lords' energy and allowed for expansion of civilization [3].

The history of wind mills would be forever changed in 1886 with the marriage of wind and electricity. Charles Brush built the first large scale wind turbine which differs from a wind mill in that it doesn't directly produce work but instead it generates electricity [3]. It was not until the 1973 oil crisis that real investment in the wind turbine industry took place. The oil crisis spurred people, and more specifically the US

government, to examine alternate energy sources, such as wind, in hopes of relieving the burden of high oil prices [1, 3]. At this point, the government began investing funds into the research and development of wind energy. For a while, wind turbines continued to boom in the US, especially California. By 1985, companies from all over the globe had installed wind turbines in California which allowed California to produce 911 MW of energy and account for 96% of the world's wind capacity [3]. The problem at this point was not the public's appeal of wind turbines but instead the lack of understanding of designing and manufacturing them. During this boom, there were countless mechanical failures and the entire boom turned into a bust by 1986 when government incentives ended. This caused a lull in wind turbine production and development in the US for at least a little while. However, around the globe, the wind turbine industry continued to grow.

It was not until the turn of the century that the US government began giving incentives once again to renewable energy sources. In 2007, when the "green initiative" really started, over $1.1 billion were given in incentives to spark an immense growth of wind turbines across the nation [5].

Wind power is the fastest growing source of energy in the world [6]. Table 1.1 which was created from data that was collected from Refs. [7, 8] shows global statistics of wind power generation in the major wind power producing countries.

Table 1.1: Wind Power Global Statistics

Country	Total MW Wind Power Capacity	2011 Installed MW Wind Power	Wind Power Capacity Penetration
China	62,364	17,631	1.6%
United States	46,916	6,816	2.9%
Germany	29,075	2,007	7.6%
Spain	21,673	1,050	16.4%
India	16,266	3,300	4.0%
France	6,836	875	3.0%
Italy	6,733	950	3.0%
U.K.	6,470	1,092	4.2%
Canada	5,265	1,298	2.5%
Portugal	4,302	315	18.0%
Denmark	3,952	206	28.0%

At the turn of the century, the US was leading the way in wind energy production but, over the last few years, many other countries have progressed quite rapidly in their own wind power programs. Between 2007 and 2009 the US was still the number one nation in new wind power capacity additions each year with nearly 30% of the world's new wind power. However, as of the last few years, China has taken over as the country installing the most wind power capacity each year. In 2011 China added 17,631 MW wind turbine power whereas the US only added 6,816 MW. The 6,816 MW contributes to only 16% of the world's new wind power capacity additions. Thus, even though the US has been surpassed as the leading nation for new wind turbines, it still possesses the second most of any country in cumulative wind power capacity at 46,916 MW. China

still produces the most with 62,412 MW of power based on data gathered at the end of 2011 [8].

Wind power capacity penetration, which looks at a specific region's installed wind power capacity and relates that to the region's overall energy capacity [9], is a good quantity to inspect in order to judge how much a region or a country is using wind power as compared to other methods of energy production. In this arena, the US is still far behind many countries with only approximately 2.9% of energy production coming from wind power. These numbers put the US thirteenth on the list falling far short of nations like Denmark at 28%, Portugal at 18%, Spain at just over 16%, Ireland at 18%, and Germany at 7.6% [6].

1.3: Problem Overview

General Electric's (GE) goal is not to simply be competitive in the wind turbine industry but to be the best. To achieve this objective, overcoming the noise issue is towards the forefront of their goals. Siting of a wind turbine is extremely important when it comes to eliminating noise perceived by the public. However, as wind power industry continues to grow, wind turbines are moving closer and closer to residential areas. As a result, choosing the location of a wind turbine is becoming less effective. Other steps must be taken to reduce the amount of noise produced by the wind turbines themselves.

1.3.1: Wind Turbine Noise

According to Webster's Dictionary the word 'noise' is a "sound: especially: one that lacks agreeable musical quality or is noticeably unpleasant." or "any sound that is undesired or interferes with one's hearing of something [10]." Based on these definitions, it can be seen how noise is really a subjective issue. There is no absolute measure of noise like there is for sound. There are many factors that determine whether a sound is viewed as noise or not. The duration of a sound, its consistency, and other background sounds are just a few of the factors that play an interconnected role to determine whether sound is seen as noise.

Wind turbines generate both aerodynamic and mechanical sound. Aerodynamic sound is produced by the air flowing around the blades [1]. Many studies have been conducted in hopes of understanding this aerodynamic sound better in order to overcome its effects. These studies have looked at such phenomenon as leading edge separation, surface boundary layer, tip vortex, trailing edge flow, etc. [11]. Over the years, the advancement in the design of the blades have indeed effectively reduced the amount of aerodynamic sound produced.

Mechanical sound, though not the primary contributor to the noise produced, is still significant. This sound is primarily generated by the gearbox [4] whose vibrations are propagated into the surrounding air. Figure 1.1 was provided by GE and used with its permission. It shows one way in which the sound propagates.
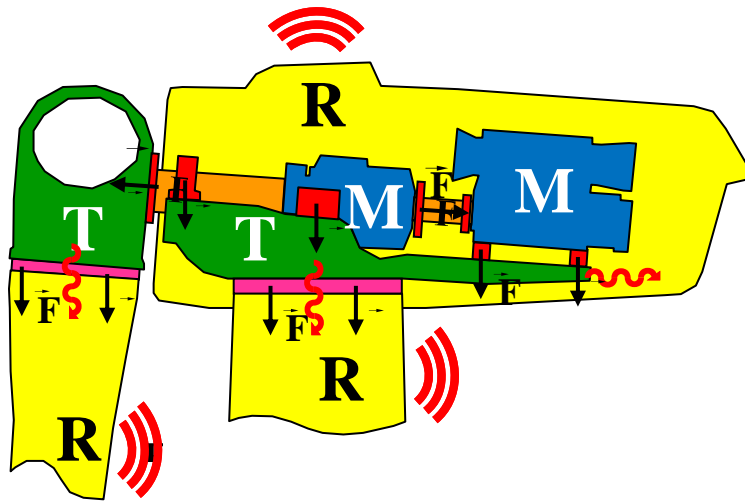
Figure 1.1: Wind Turbine Sound Propagation

The two mechanical components (denoted by 'M') are the gearbox and the generator. These are the two dominant mechanical components within a wind turbine, which can produce either air-borne noise or structure-borne noise [4]. Air borne noise is when the sound produced is propagated through the air and escapes the nacelle (the housing) through any openings. Structure-borne noise occurs when the gearbox produces forces which are then transmitted into other structural components of the wind turbine and radiated through the mainframe into the tower, the blades, or the nacelle. These are the main two paths that noise generated from the gearboxes takes to propagate into the surrounding area.

1.3.2: Noise Produced by Gears

Noise from the gearbox is caused by a force variation within the gears. This then causes vibrations which are transmitted into other components or into the air. These

vibrations are primarily due to inaccuracies in the gear mesh. The force variation is a result of the transmission error (TE) that occurs within gears. In simple terms, TE is the difference between where a gear should be and where it actually is. The angle of the input shaft is measured and subtracted from the position that it should ideally be. For an ideal gear there is no TE because the forces never vary.
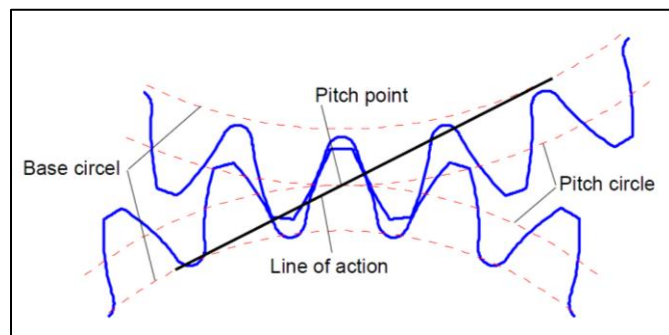
Figure 1.2: Gear Pairing Showing Line of Action (Credit Henrickson [12])

Figure 1.2 shows the ideal meshing of two gears. The line of action represents the path that a string would have if it were tightly wound around the base circle of one gear and then connected to the tangent line of the mating gear base circle. For an ideal gear mesh, there will only be contact between the two teeth at points on that line. When this is the case, the origin of the contact forces and their direction lie on that line as well. In an ideal case, there is no force variation because the force vectors always lie on the line of action.

Realistically though, no gear mesh is perfect. Manufacturing errors of the gear teeth profile will cause very slight displacements. These displacements, may be small, but still have an effect on the contact location. When the contact location is altered from where it ideally should be, the forces produced vary as well. This force variation causes vibrations to be transferred.

When gears are under load there is going to be deformation that occurs not only in the shafts, but also in the gears, and more specifically within the gear teeth. As Smith points out [13], the gear teeth themselves are elastic and experience significant deflections. These deflections are increased when load increases and the rpm of the gears increase. The shafts experience torsional deformation when a torque is applied. The main body of the gear is not perfectly stiff either. All of these small errors influence the TE that is within a gear mesh. This displacement is typically less than 10µm, but no matter how small though, it still causes a force variation. These variations are cyclic in nature, occurring every time a new tooth passes through the mesh as seen in Figure 1.3 [14].
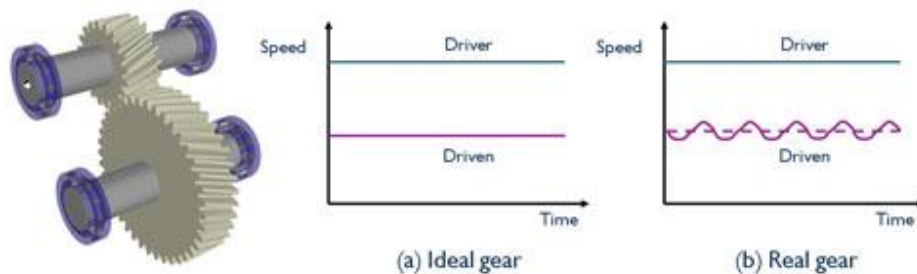
Figure 1.3: Transfer of Motion for (a) an Ideal Gear and (b) a Real Gear

This self-excited vibration is then transmitted into the housing. It is these vibrations in the housing that transmit the noise into the air or into other structures as seen in Fig. 1.1.

1.3.3: Previous Methods to Reduce Noise

After noise is generated by the gearbox, and propagated through the nacelle or tower, it then reaches the ears of people. This is where it becomes an issue. Many steps have been taken over the years to reduce the amount of noise produced by the gearbox and generator. More precise manufacturing techniques to produce more accurate teeth profiles will reduce the TE within the gear meshing, which, in turn, will reduce the undesired forces. If these forces are reduced, vibrations caused by the gearbox will be reduced as well. Different vibration absorbers have also been used in the mounting of the gearbox to dampen the vibrations and hinder the transfer of vibrations to other components of the wind turbine [4, 11]. One other step that can be taken is to insulate the inside of the nacelle to capture the noise before it escapes [4]. These are all passive methods of vibration control that deal with the design of the structures or the mechanical components.

1.4: Research Team and Plan

This section will lay out the plan of work for this research and briefly describes how several GE employees contributed and played a part in this research.

1.4.1: Project Team

This is a bulleted list of all the people who contributed to this project and what their specific role or contribution to the project.

- Kurt Goodwin – Sponsoring Engineering Manager

- Priyangu Patel – Project Manager

- Mohammad Daqaq – Clemson Professor and Project Advisor

- James Madge – Project Consultant

- Munishwar Ahuja – Project Consultant

- Mike Garry – Project Engineer

- Matthew Evans – Project Engineer

1.4.2: Thesis Objectives and Organization

The main goal of this research is to reduce the noise produced by the gearbox. In order to do this, the frequencies that create the greatest vibrations will need to be identified. To this end, a 3-D model of the gearbox is created and analyzed. Then passive methods of vibration control will be investigated to eliminate or decrease the vibrations caused by these trouble frequencies.

The following is a layout of the material within this thesis.

- Chapter 2: In this chapter, we describe and analyze the GE Compact Gear Drive Train (CGDT) wind turbine. This will help provide better understanding

of the research and therefore the rest of the thesis. We take a look back at how the CGDT test stand was set up to acquire data and then store the data in waterfall plots. The use of this data is a driving force in this research because it is used as a reference for verifying the created 3-D model's accuracy. We examine the process of taking the stored data, analyzing and compiling it in such a manner that it can be used for a three-level comparison of the 3-D model to the actual experimental data. The three characteristics that are used for the three-level comparison are the dynamic response orders of the CGDT gearbox housing, the natural frequencies of the CGDT gearbox housing, and the mode shapes of the CGDT.

- Chapter 3: It is within this chapter that the 3-D modeling begins using the FEA analysis software known as ANSYS. This chapter lays out the set up process, which includes the creation of the 3-D model. It also lists and justifies the assumptions that were used. Modal analysis is performed; the results are presented and compared to the experimentally collected data that was presented in Chapter 2. Based on the comparison, the assumptions were re-visited. The approach as a whole was re-assessed to figure out another route for analysis.

- Chapter 4: A more comprehensive analysis approach using MASTA, a design and analysis software specifically for systems involving gears, is presented. A model of the entire test stand is presented and modified. The model's

boundary conditions, and the assumptions behind them, are discussed. The results of the predicted orders, excitation frequencies, and mode shapes of the gearbox are shown. These are then compared to experimental data showing a strong correlation for both the orders and excitation frequencies and inconclusive comparison of the mode shapes.

- Chapter 5: This portion of the thesis will briefly recount what has been accomplished within this project and the conclusions that came about as a result. Several comments will be made as to how this research, and the results obtained through it, will help future work in this area, specifically within GE.

CHAPTER 2: GENERAL ELECTRIC'S 2.5 MW CGDT GEARBOX

In this chapter, we describe and analyze the GE Compact Gear Drive Train (CGDT) wind turbine. This will help provide better understanding of the research and therefore the rest of the thesis. We take a look back at how the CGDT test stand was set up to acquire data and then store the data in waterfall plots. The use of this data is a driving force in this research because it is used as a reference for verifying the created 3-D model's accuracy. We examine the process of taking the stored data, analyzing and compiling it in such a manner that it can be used for a three-level comparison of the 3-D model to the actual experimental data. The three characteristics that are used for the three-level comparison are the dynamic response orders of the CGDT gearbox housing, the natural frequencies of the CGDT gearbox housing, and the mode shapes of the CGDT.

2.1: Overview

GE is developing a new compact gearbox which has the generator mounted directly to the rear of the gearbox. This eliminates the need of a flexible coupling between the gearbox and generator and decreases the space that is necessary to house the gearbox/generator combination.
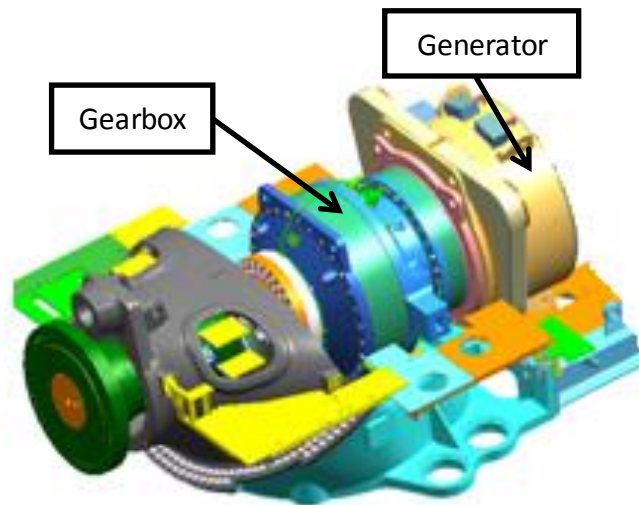
Figure 2.1: 3-D Model of CGDT Gearbox with Generator

Figure 2.1 was provided by GE to show this new CGDT design. This design is a 2-stage, medium speed gearbox that acquires the input from the rotor blades and transforms that energy to power the generator. The input from the rotor to the gearbox is one of high torque and low rpm. The two stages of the gearbox transform this input into high rpm and low torque to run the generator. Each stage of the gearbox is a

planetary stage which consists of a ring gear built into the housing of the gearbox, planet gears, and a sun gear acting as the input gear. The first stage has four planetary gears, a single internal ring gear, and an input sun gear. The second stage is very similar except that it only has two planetary gears.

2.2: Test Stand

This section explains the layout of the test stand setup used in the experiments, the different sensors used throughout the testing cycles, and the data collected. The reader should keep in mind that all of the testing and data collection was done prior to this project by GE. However, it must be presented because of its critical role within the project.

Figure 2.2 depicts the test stand at GE's facility with the CGDT mounted and prepared for a test run.
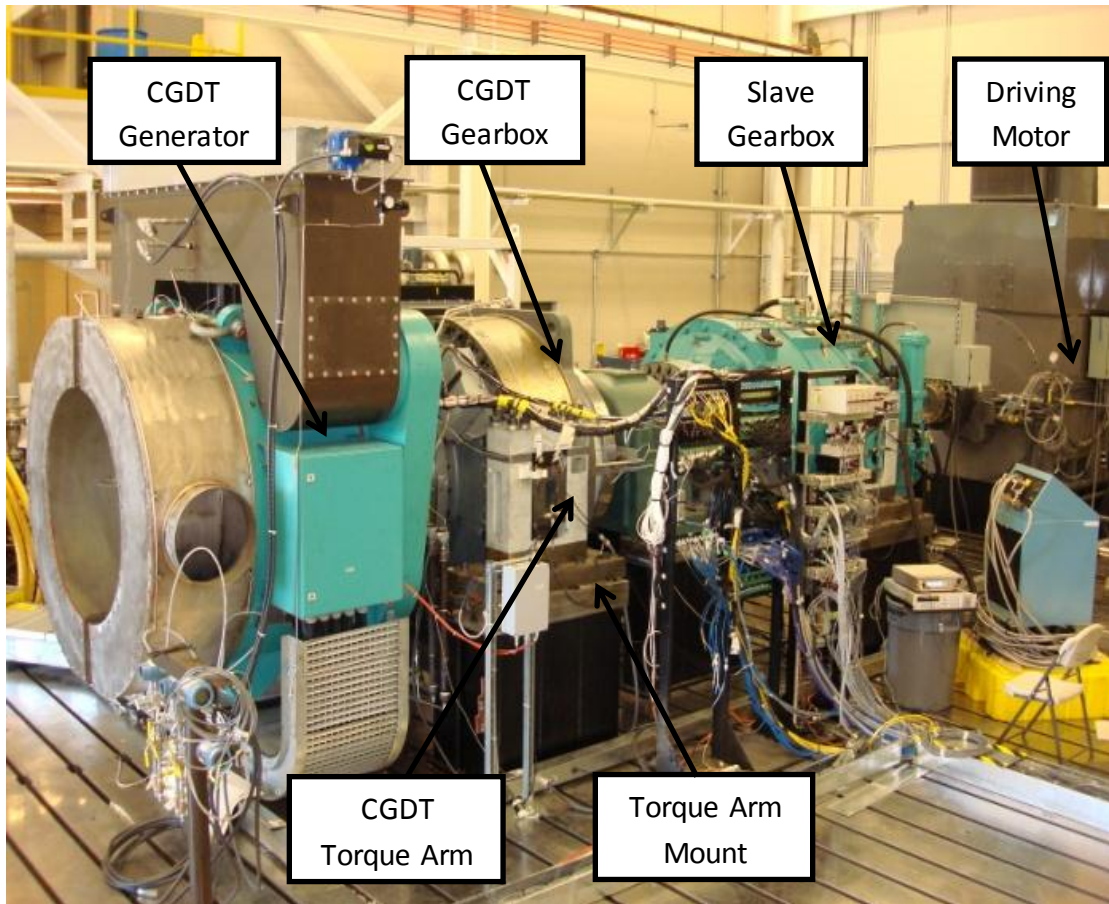
Figure 2.2: GE's CGDT Test Stand

The driving motor applies an input of low torque and high rpm into the slave gearbox. To replicate the input that the CGDT would see in the field, the slave gearbox is mounted backwards, therefore converting the input from the driving motor into high torque and low rpm output. The output is then transferred through the main shaft to the CGDT which transforms it into low torque and high rpm, and supplies to the generator. As can be seen in Figure 2.2, each torque arm (TA) on the gearbox housing is

supported by TA mounts. These TA mounts contain elastomeric material that dampens the vibrations caused by the gearbox.

2.3: Data Collection and Analysis

2.3.1: Waterfall Plots

A group of five tri-axial accelerometers were strategically positioned on the CGDT gearbox housing. Table 2.1 lists these five accelerometers and gives a brief description of where they were located.

Table 2.1: Sensor Location Description

Test Stand Accelerometer Number	Sensor Location Description
65001	Front Case: At 12 o'clock on the outside surface
66001	Torque Arm: on the right TA when looking Down Wind
66002	Torque Arm: on the left TA when looking Down Wind
68002	Aft Case: at 11 o'clock on the outside surface
68001	Aft Case: on the outside surface between the upper left and lower right pockets, as viewed from down wind

Collected data from these sensors were stored in the form of waterfall plots. These waterfall plots are 3-D plots that depict the variation of the response amplitude with the gearbox excitation frequency and the generator rpm. They are produced when the amplitude response curves are plotted across the frequency spectrum (0-1,000Hz). This is done multiple times as the rpm is increased. For every accelerometer, waterfall plots

are produced for each direction. Therefore, the axial, horizontal, and vertical directions can be analyzed for all five accelerometers. There are two sets of waterfall plots, one in terms of acceleration and the other in terms of displacement. The acceleration waterfall plots become unreliable at low frequencies due to interference issues. To remedy this, displacement waterfall plots are created to observe only the low frequency range (0-50Hz). The process of transforming the accelerometer signal into displacement eliminates a great deal of the external interferences, thus producing a much cleaner plot. In all, thirty waterfall plots are produced.
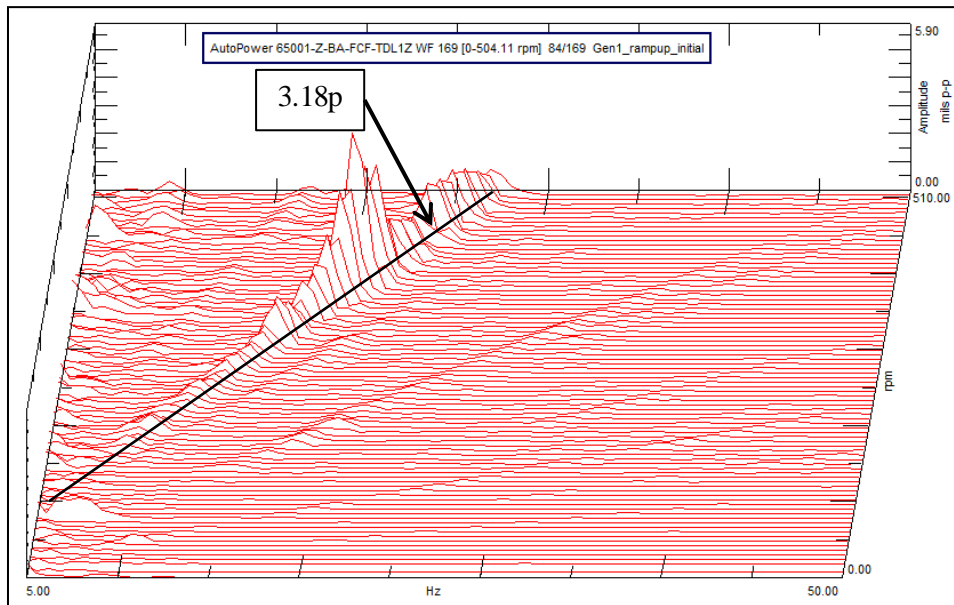
Figure 2.3: Waterfall Plot of Horizontal Displacement from Accelerometer 65001
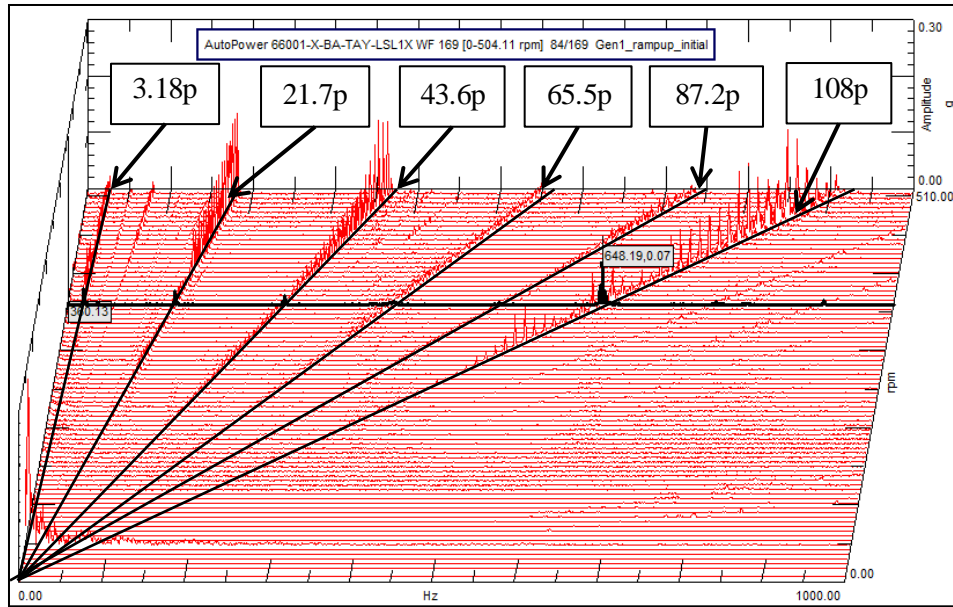
Figure 2.4: Waterfall Plot of Axial Acceleration from Accelerometer 66001

Figure 2.3 and Figure 2.4 depict what these waterfall plots look like by showing a displacement waterfall plot (Figure 2.3) and an acceleration waterfall plot (Figure 2.4). The purpose for acquiring these plots is to give us experimental data by which future models can be compared to. We specifically want to look at dynamic characteristics that determine the behavior of the gearbox.

2.3.2: Orders

To achieve this goal, the first, and, most basic characteristic of interest to us is the orders of the gearbox. The equation for an order (p) is given by:

$$p = \frac{f * 60}{rpm} \tag{2.1}$$

An order here is essentially a ratio between the gearbox housing frequency (f) and the generator rotations per minute (rpm). Since a gearbox's rpm is dependent upon the gears and their tooth ratios, large amplitude motion, when excited, do not occur at one frequency, but, rather, along a line of frequencies depending on the rotational speed. This line of frequencies, also shown clearly in Figs. 2.3 and 2.4, is known as the order line. Obtaining the orders present within the test data provides a quick and simple comparison to confirm a model's accuracy on a basic component level.

Obtaining the orders from the waterfall plots is a straightforward process. By inspecting Fig. 2.4, it can be observed that the x-axis is the frequency and the y-axis is the rpm. Equation (2.1) is a linear equation and therefore over a range of rpm and frequency, the order lines will be linear as well. These order lines are calculated by picking off the amplitude spikes and determining the frequency and rpm at which that spike occurred. Those two values would simply be input into Equation (2.1) to calculate the order. For example, looking at Fig. 2.4, the horizontal line was added by using the LMS Test Lab Data Software where the waterfall plots were stored. Within this program the plots could be accessed and individual lines could be created to show the rpm, frequency, and amplitude of a specific point. At that peak it tells that the frequency is 648.19 Hz and the line intersects the y-axis at 360.13 rpm. Plugging those two values into Equation 1 produces an order of 108 p. This same process for determining the orders was performed for all of the significant amplitude responses in all thirty of the waterfall plots. A compilation of all significant order values is provided in Table 2.2.

Table 2.2: Experimental Data Orders

Orders	
1st	3.18
2nd	21.83
3rd	43.66
4th	65.49
5th	87.32

All five of these orders can be seen in Fig. 2.4. Also it may be of value to note that the 108p is not included in this table based on GE's previous knowledge that the 108p results from the generator's vibration and not from the gearbox. Since the generator is outside the scope of this research, the 108p is ignored in Table 2.2 and throughout the rest of this research.

2.3.3: Excitation Frequencies

Another aspect of the waterfall plots that will be examined are the dominant excitation frequencies. It is those frequencies within the frequency spectrum that, when they match the natural frequencies of the housing, cause the largest amplitude response. We want to find these frequencies because they ultimately produce the most noise. These waterfall plots are ideal for identifying them because they will have the largest amplitude response and will, oftentimes, be observed within multiple orders. A closer inspection of the waterfall plot shown in Fig. 2.3 (reproduced in Fig. 2.5) will make this more clear.
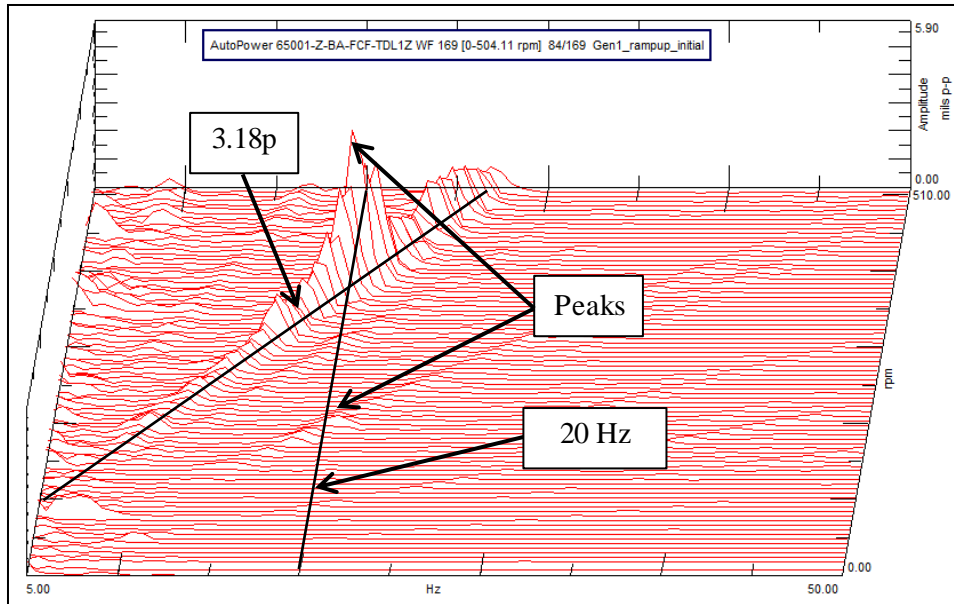
Figure 2.5: Waterfall Plot of Horizontal Displacement from Accelerometer 65001 with Peaks Shown

Figure 2.5 shows a waterfall plot that clearly contains a large amplitude spike. This spike occurs at 20Hz, therefore a line for 20Hz is drawn across the entire rpm range. This one frequency creates spikes on two separate orders. Granted there is only one large spike that occurs on the 3.18 order but the other spike that is pointed out is larger than any other amplitude response along its order. Using this plot, it was determined that the 20Hz is an excitation frequency that matches the natural frequency of the housing. The same process was then performed on all thirty waterfall plots to obtain the trouble frequencies. The acceleration waterfall plots were difficult to analyze in this way. This is due partly due to the difficulty in pin-pointing peaks and partly because it was difficult to tell if any peaks did occur within the range shown. It was determined at this point

that the acceleration plots would be examined, but only the general trends of these plots would be compared and discussed in the future. The trouble frequencies seen within the displacement waterfall plots are listed in Table 2.3.

Table 2.3: Displacement Sensors Frequency Comparison

Trouble Frequencies	
Test Frequency [Hz]	Primary Direction
8	Axial, Vertical, and Horizontal
15	Vertical and Horizontal
20	Axial, Vertical, and Horizontal
27	Axial

Because a single waterfall plot is for a specified direction, the primary direction of the movement for a given trouble frequency could be deduced. The above information will help when comparing results from a modal analysis on a created model to obtain the natural frequencies.

2.3.4: Laser Channel Sensors

The test stand set up also included laser sensors that measure the displacement of a point in all three degrees of freedom. These are very sensitive lasers that can detect displacement as small as 0.005mm. There were four of these sensors mounted onto the test rig to collect data. One sensor located on each of the two TAs of the CGDT and on each of the two TAs of the slave gearbox. Figure 2.6 shows an overhead view of the

slave gearbox and the CGDT gearbox with the laser sensors located at TA 1, TA 2, TA 3, and TA 4.
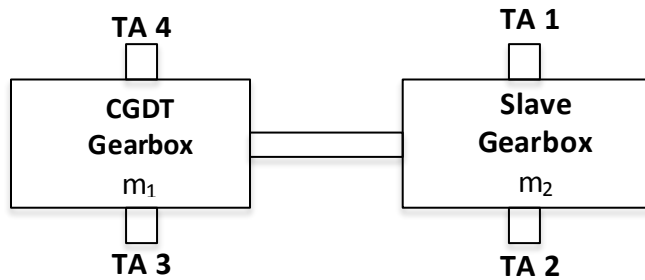
Figure 2.6: Test Stand Diagram with Torque Arms Labeled

With the laser sensors mounted on the TAs, a ramp up test was performed and data was collected. Table 2.4 is the data that was acquired by these lasers. Whenever a displacement was detected, the frequency, order, and rpm were also recorded and are shown in Table 2.4 as well.

Table 2.4: Laser Channel Data

Laser Channel												
Freq, speed, order mode	Vertical (mm)				Lateral (mm)				Axial (mm)			
	TA 3	TA 4	TA 2	TA 1	TA 3	TA 4	TA 2	TA 1	TA 3	TA 4	TA 2	TA 1
1 2 Hz 0.5p 240rpm	-	-	-	-	0.03	0.025	0.03	0.03	0.03	0.03	0.03	0.03
2 9.7 Hz 3.2p 182rpm	-	-	-	-	-	-	0.02	0.02	0.01	0.015	0.02	0.02
3 18.4 Hz 3.2p 345rpm		-	-	-	0.025	0.025	-	-	-	-	-	-
4 20.5 Hz 3.2p 385rpm	0.015	-	-	0.025	-	-	0.025	0.025	0.04	0.025	0.05	0.035
5 23.4 Hz 3.2p 438rpm	0.02	-	0.03	0.02	0.02	0.01	0.02	0.025	0.02	0.015	0.07	0.03
6 27.3 Hz 3.2p 505rpm	-	-	-	-	-	-	-	-	0.065	0.02	-	-
7 40.8 Hz 6.4p 383rpm	0.01	-	-	-	-	0.005	-	-	-	-	-	-

A dash symbol within a box indicates that there was no movement detected. A value indicates the measured movement at the specified mode. The modes that were picked up by these sensors were intriguing because they do not align with the trouble frequencies from Table 2.3. These laser sensors, however, do not necessarily describe the movement of the gearbox as a whole, but instead simply the movement of the TAs. As such, it is possible that the torque arms are excited at more frequencies than the gearbox as a whole. And that these excitations are just not as significant as the ones shown in Table 2.3. The waterfall plots support this idea. Taking the same waterfall plot from Fig. 2.3 and analyzing it more closely with respect to modes 2 and 3 from Table 2.4, we obtain Figure 2.7 and 2.8.
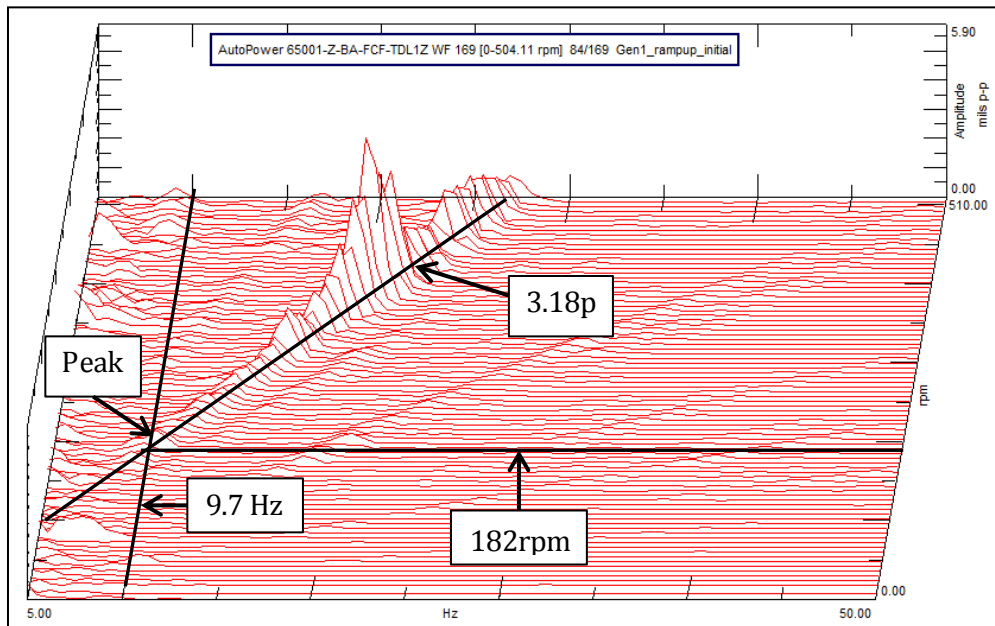
Figure 2.7: Waterfall Plot of Horizontal Displacement from Accelerometer 65001 Showing Mode 2

Figure 2.7 shows mode 2 at 9.7Hz and 182rpm. These two lines are drawn and where they intersect the 3.18p line a peak can be seen. This indicates that there is some excitation at the points.
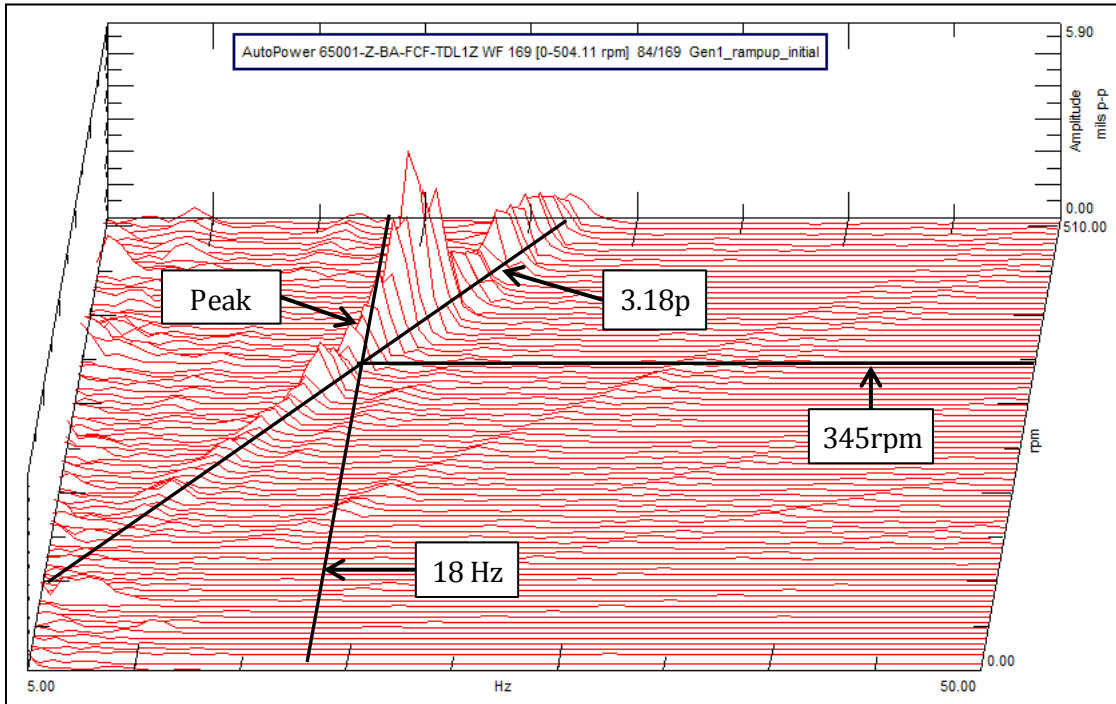
Figure 2.8: Waterfall Plot of Horizontal Displacement from Accelerometer 65001 Showing Mode 3

Similarly Fig. 2.8 examines mode 3. It has a frequency of 18Hz at a speed of 345rpm. When those lines are drawn they intersect on the 3.18p line. At this intersection point, there is a peak in the response, which again indicates a possible source for the excitation.

These two figures show that the modes captured by the laser sensors were seen within the waterfall plots. The reason they were not in Table 2.5 as a trouble frequency is because, compared to other amplitude spikes, they are relatively small. With all of that said, Table 2.5 is extremely important, because it gives us insight into the mode shape of the CGDT gearbox.

2.3.5: Mode Shape

The third and final dynamic characteristic which will be used for comparison is the mode shape of the CGDT gearbox. Out of the three characteristics, this is the most difficult to determine based on experimental data. It is, however, the most comprehensive comparison that can be done. The mode shape defines the displacement of the gearbox housing. The deformation of components will contribute to the mode shape. By referencing Fig. 2.6 and the data in Table 2.4, the mode shapes will be determined. To interpret the data from Table 2.4, the movement detected by each laser sensor must be analyzed. By examining mode 1 we see that there is movement in all of the TA but only in the axial and lateral directions. At this mode of vibration, the TAs do not undergo any vertical movement. Based on this analysis, a mode shape can be deduced. Mode 1 produces a rigid body rotation of the system about the main bearing as depicted in Fig. 2.9.
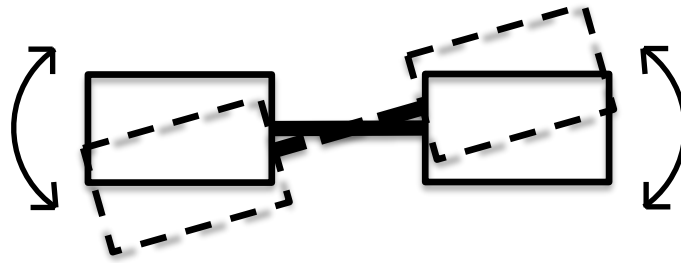
Figure 2.9: Diagram of Observed Mode Shape at 2Hz

Figure 2.9 is a simple diagram of the test stand showing the two gearboxes connected by the main shaft. The solid lines depict the original position and the dashed lines outline the transformed position with the arrows showing the direction of motion. Similarly by examining mode 2, it can be determined that none of the TAs move vertically. TA 1 and TA 2 move laterally. This indicates that the slave gearbox moves laterally. At the same mode though all TAs move axially. This means that both the CGDT and the slave gearbox are moving laterally. It is in this manner that the mode shapes were determined from the test stand and Table 2.5 is created.

Table 2.5: Laser Channel Mode Shape Description

	Laser Channel	
Mode	Frequency, Order, Speed	Mode Shape Description
1	2Hz, 0.5p, 240rpm	Rigid body rotation of the system about the main bearing. Gearboxes are laterally OUT of phase, axially IN phase.
2	9.7Hz, 3.2p, 182rpm	Slave gearbox only lateral mode. Axial twist motion in both gearboxes.
3	18.4Hz, 3.2p, 345rpm	CGDT only lateral bending/swaying mode. Coupled with axial movement of all TAs.
4	20.5Hz, 3.2p, 385rpm	Slave only lateral bending/swaying mode. Coupled with axial movement of all TAs.
5	23.4Hz, 3.2p, 438rpm	Laterally in phase, CGDT leads slave by 90 degrees. Axially out of OUT of phase, CGDT leads by 90 degrees.
6	27.3Hz, 3.2p, 505rpm	CGDT only axial mode, in phase.
7	40.8Hz, 6.4p, 383rpm	CGDT TA 4 only mode.

2.4: Conclusion

At this point the test stand's data has been analyzed and the orders, trouble frequencies, and mode shapes have been determined. The five orders listed in Table 2.3 should appear in any future model. If this is not the case, then there is an inaccuracy with the model's gear ratios. Also, future models should possess large excitations at the trouble frequency values listed in Table 2.4. If there is a discrepancy within this comparison, then it can be concluded that there is an error with the interactions of the gearbox components. Ultimately, the mode shapes listed in Table 2.5 will be used as a

reference to confirm whether or not a model deforms in the same manner. These are the three levels of comparison that will be used throughout this project. Having multiple data sets and procedures will hopefully permit comprehensive validation of any developed computational models.

CHAPTER 3: MODAL ANALYSIS OF THE GEARBOX HOUSING

It is within this chapter that the 3-D modeling begins using the FEA analysis software known as ANSYS. This chapter lays out the set up process, which includes the creation of the 3-D model. It also lists and justifies the assumptions that were used. Modal analysis is performed; the results are presented and compared to the experimentally collected data that was presented in Chapter 2. Based on the comparison, the assumptions were re-visited. The approach as a whole was re-assessed to figure out another route for analysis.

3.1: Overview

This chapter marks the beginning of actual creation of the 3-D models. A working flow chart was created to give a big picture overview of the necessary steps within this project.
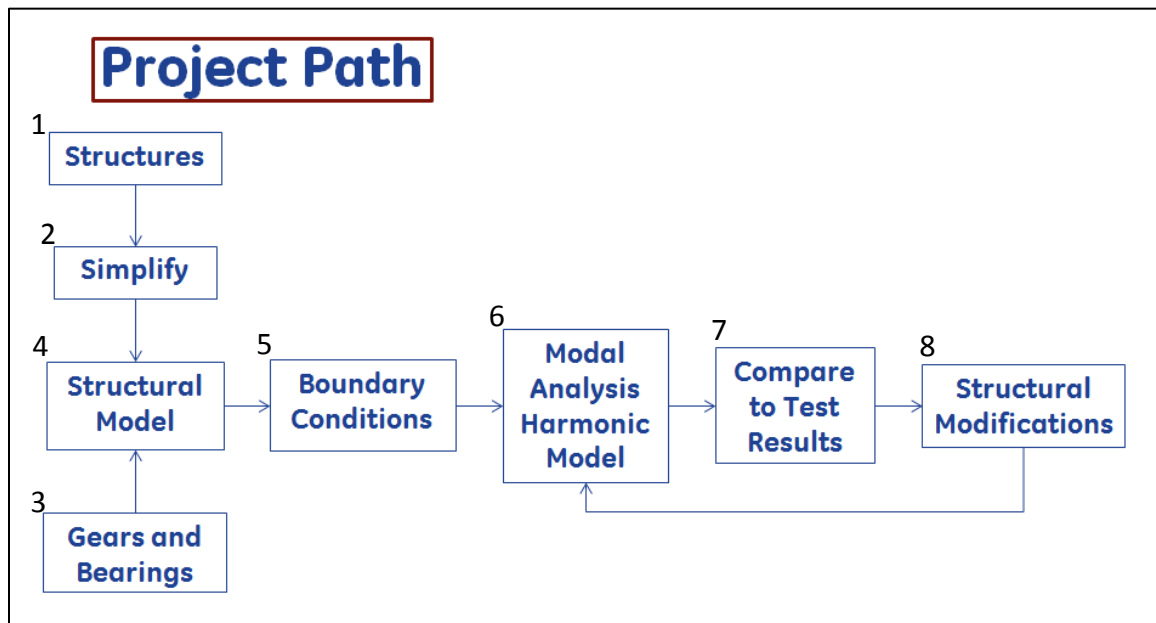
Figure 3.1: Project Path Flow-Chart

Figure 3.1 shows the final flowchart that was used as a reference to keep the research on track and was revisited several times to modify based on new information.

Boxes 1-3 are all inputs into box 4, representing the final 3-D model. Box 1 refers to the selection of the components of the gearbox that will be analyzed. Box 2 signifies any simplification of the chosen components. This applies to the simplification of

components to save computational time. Finally, Box 3 represents the influence of the gears and bearings. In this portion, the influence of these components is accounted for. The first three boxes all go into making the 3-D model, box 4. From there, boundary conditions (BC's) will then be applied in Box 5. After that, Box 6 represents the actual analysis performed on the model. The results are then compared to the experimental data (Box 7) for accuracy. If shown to be accurate, the model would then be modified to eliminate the resonant interactions. The analysis would be run once again and the results analyzed and compared to the experimental data in order to see if the resonance amplitude were reduced or eliminated. Getting to this point is the ultimate goal of the project.

Within this first part of the project an assumption was made in order to help expedite the process. We assumed that the gear mesh would only transfer energy to the gearbox housing if the excitation frequencies correlate to a natural frequency present within the housing. In other words, there is only a one-way interaction between the gears and the housing. The gear acts as an excitation and the housing responds to it, but the modal frequencies of the housing are not affected by the gears themselves. This assumption was made due to the relatively small mass of the internal components and gears. This enables us to eliminate the internal components all together and analyze the housing components only. Performing modal analysis to obtain the natural frequencies of the housing is a simple and quick process. These results will confirm whether or not the housing possesses natural frequencies that match the trouble frequencies seen in

Table 2.3. If this turns out to be the case, then the process can move onto making modifications to the housing components to shift these natural frequencies very quickly. The first step to accomplish this is to create a 3-D model of the housing.

3.2: 3-D Model Creation

The modeling software, NX, was used in this part of the project to model the main components of the housing for the gearbox. These main components are the front case, the aft case, the TA case, the first (1st) stage ring gear, and the second (2nd) stage ring gear. Figure 3.2 shows a model of the CGDT gearbox mounted onto the bedplate of a wind turbine, while identifying these five main components.
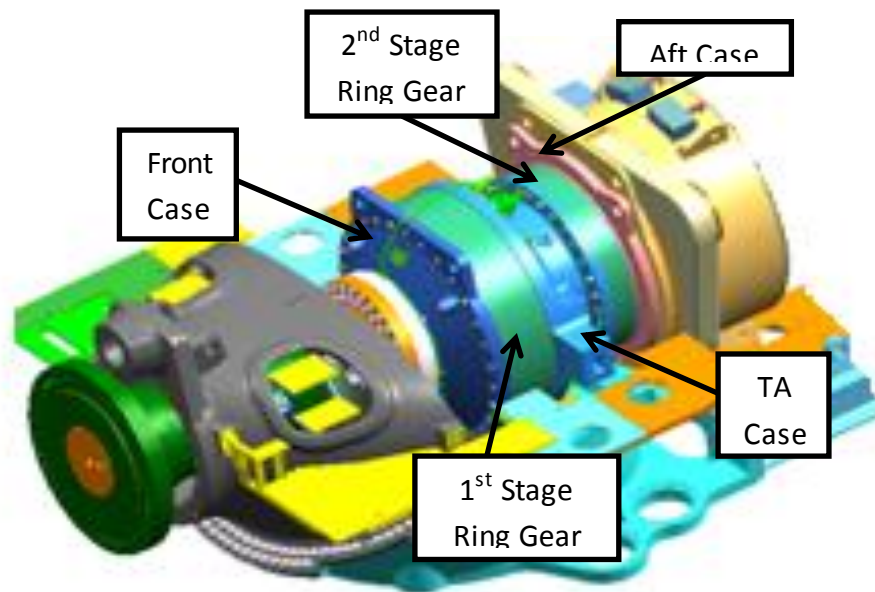
Figure 3.2: Original Gearbox within System

The front case shown in Fig. 3.3 is at the front of the gearbox and is mounted directly to the main shaft. This is where the input from the rotor enters into the gearbox.
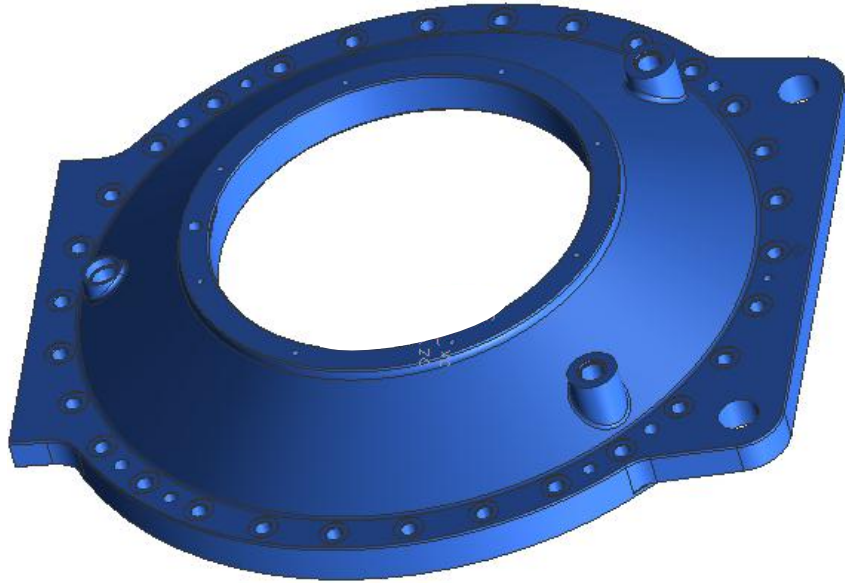
Figure 3.3: Original Front Case of Housing

The 1st and 2nd stage ring gears are nearly identical, just different size. These ring gears are seen in Figure 3.4. It would be beneficial to keep in mind that typically there are teeth on the inside portion of the rings but they have been hidden so as not to disclose any confidential information outside of GE.

| 1st Stage Ring Gear | 2nd Stage Ring Gear |
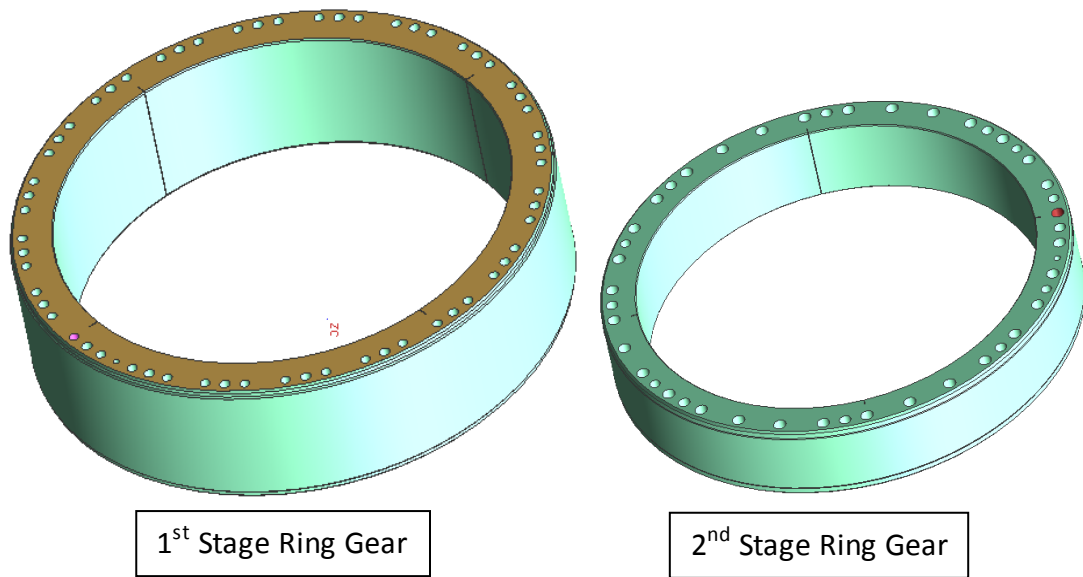
Figure 3.4: Original 1ˢᵗ and 2ⁿᵈ Stage Ring Gears (No Teeth)

The TA case, shown in Fig. 3.5, is the middle component of the gearbox housing sandwiched in between the 1ˢᵗ and 2ⁿᵈ stage ring gears. This TA case also includes the TAs that are used to mount the entire gearbox into the TA mounts which are securely bolted into the bedplate.
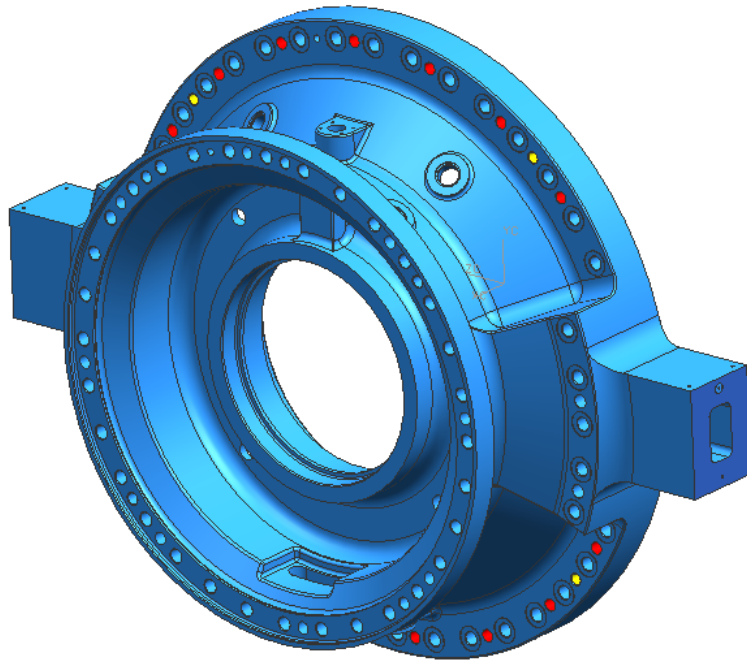
Figure 3.5: Original Torque Arm Case
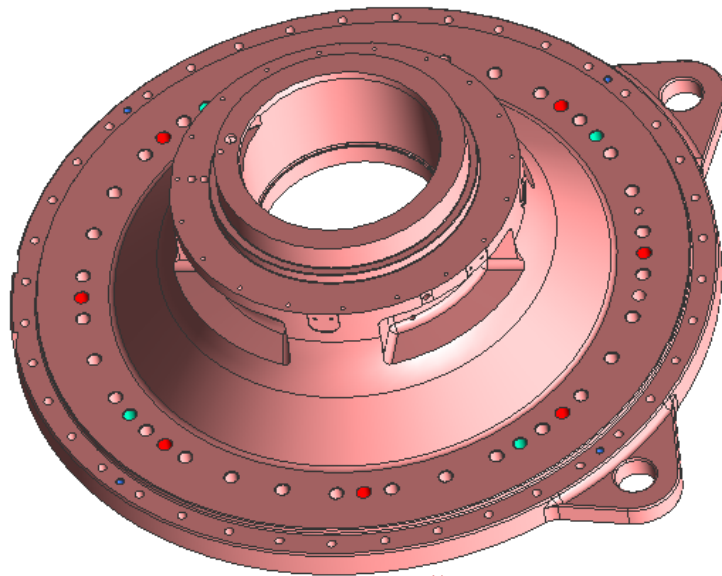
Figure 3.6: Original Aft Case

Finally, the aft case, seen in Fig. 3.6, is the last component of the gearbox and is used to attach the generator to the gearbox. These five components together form the gearbox housing. This completes the "Structures", Box 1, within the flowchart from Fig. 3.1.
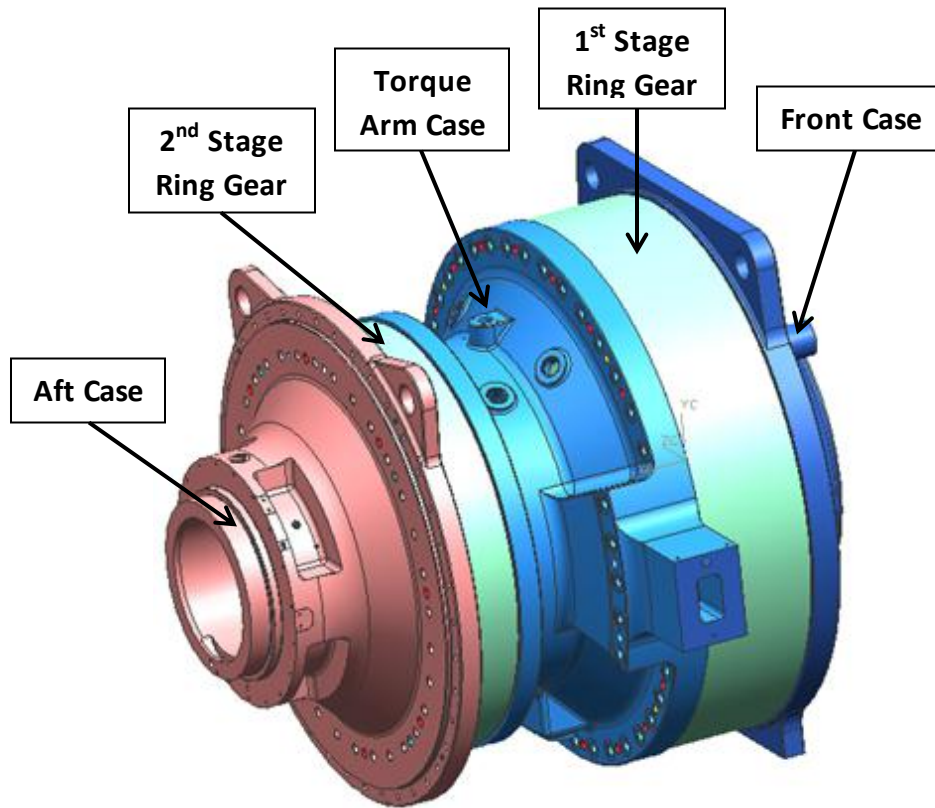
Figure 3.7: Original Gearbox Housing Assembly Model

It would be helpful to know that the material properties and the mass of each of these components is critical information to have. However, in order to respect the confidentiality agreement with GE those properties can not be presented or discussed here.

The next step in this process is the simplification of the structures. The models will be simplified for different reasons. First, the more simple the model the faster the analysis within ANSYS. Second, complexity in the models will sometimes produce inaccurate results due to meshing errors. When a mesh is applied to a model, the software is breaking the model down into smaller elements then analyzing the individual elements. The entire collection of this element analysis produces the FEA results. To simplify the models, unnecessary features of the five components of the housing will be eliminated. General Electric (GE) gave direction in this area as to what extent to simplify the model. Features that are eliminated are small fillets, chamfers, bolt holes, lifting holes, and a few other non-crucial features. These simplified components are shown in Figures 3.8-11.

Front Case / Main Shaft
Mounting Surface
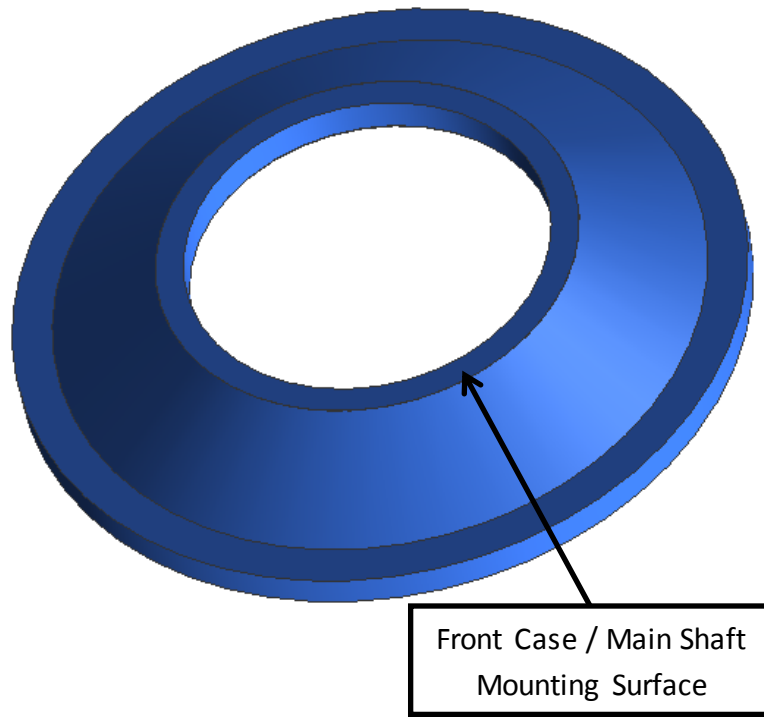
Figure 3.8: Front Case of Housing

1st Stage Ring Gear
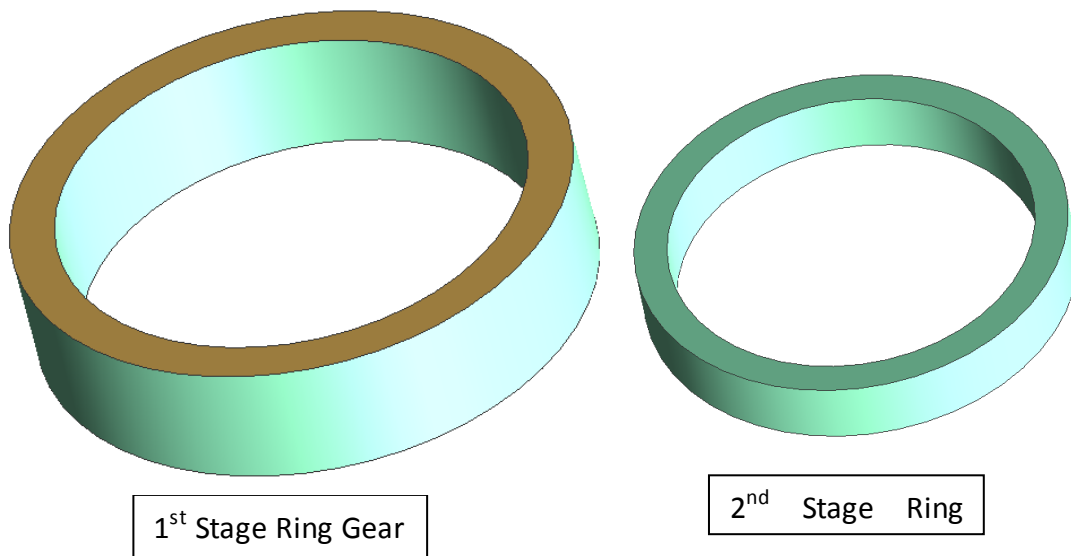
2nd Stage Ring

Figure 3.9: Simplified 1st and 2nd Stage Ring Gears
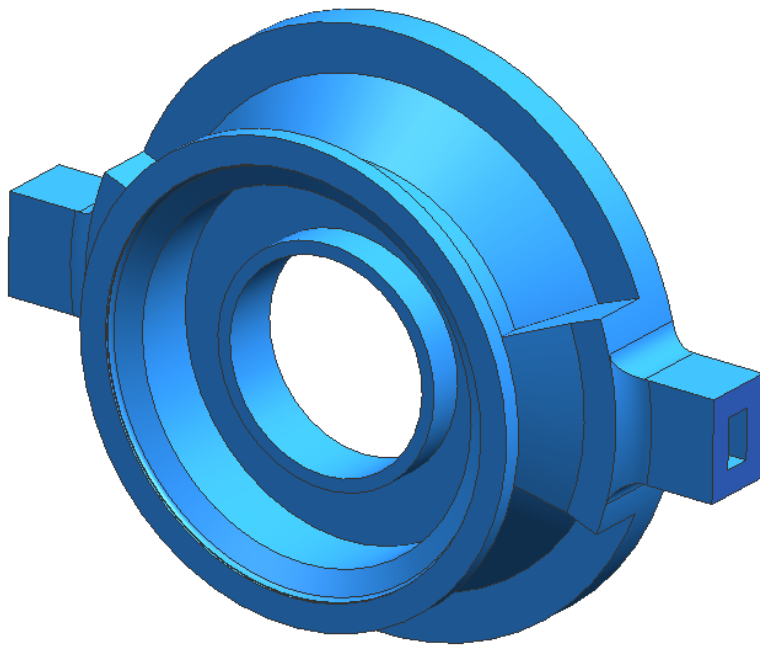
Figure 3.10: Simplified Torque Arm Case
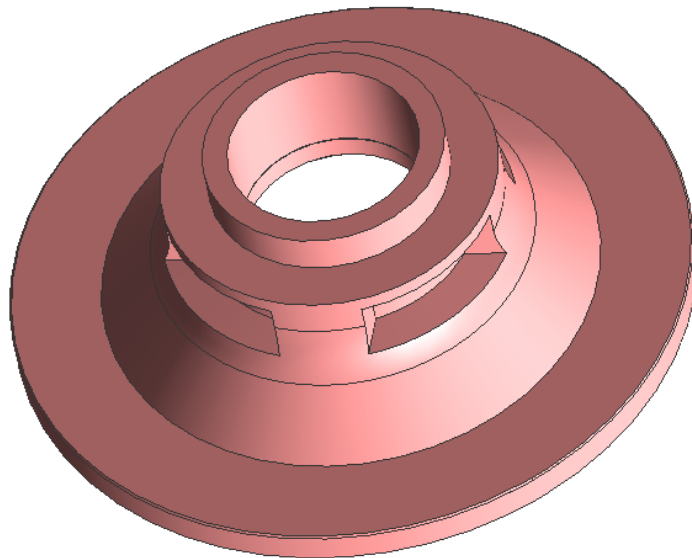
Figure 3.11: Simplified Aft Case
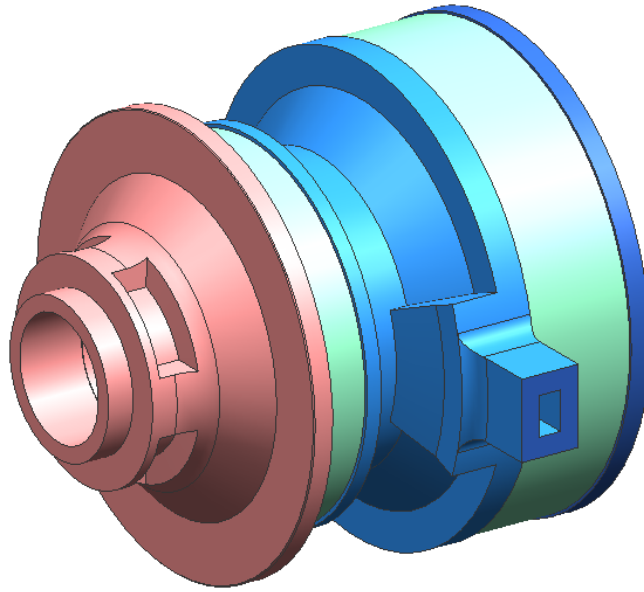
Figure 3.12: Simplified Gearbox Housing Assembly Model

We are confident that these modifications will not alter the dynamic behavior of the housing. The overall mass difference between the original housing model (Fig. 3.7) and the simplified housing model (Fig. 3.12) is less than 1 %. Also, the overall shape and size of each component has remained essentially the same. This gives us confidence in believing that the effective stiffness of the components would not be affected. Therefore, the modal frequencies will not be significantly altered.

3.3: Modal Analysis

This section will describe the set up of the model in ANSYS, the modal analysis that was performed, and the results of that analysis.

3.3.1: Boundary Conditions and Assumptions

With the simplification complete, the model is imported into ANSYS. Before the modal analysis could be performed, the proper BC's must be applied. This step corresponds to Box 5 of the flow chart within Fig. 3.1. The first set of BC's is to fix the components to each other at the interfacial surfaces. This BC is justifiable because of the large number of bolts that hold the pieces together. It is therefore safe to assume that there are no relative movements along these connecting surfaces. Another BC is applied to the main shaft/front case mounting surface shown in Fig. 3.8. This surface was fixed in space. The main shaft was very securely held in place by mounting structures. Since the main shaft is held constant, it was assumed that the front case surface mounted to the main shaft is fixed.

As can be seen in Fig. 2.2 the test stand has the gearbox TAs mounted through elastomeric mounts. These mounts are designed to dampen any movement of the TAs with an elastomer. The exact material can not be discussed but the stiffness applied in the three directions is listed in Table 3.1.

Table 3.1: Elastomeric Material Dampening and Stiffness

Elastomeric Material			
Dampening Value N/m	Stiffness Value kg/sec	ANSYS Model Axis	Test Stand Direction
1×10^6	1×10^6	X-axis	Axial
2×10^8	2×10^8	Y-axis	Vertical
1×10^6	1×10^6	Z-axis	Horizontal

For these mounts the vertical direction (Y-axis) was assumed to be more highly damped and stiffer than the axial (X-axis) and horizontal direction (Z-axis).
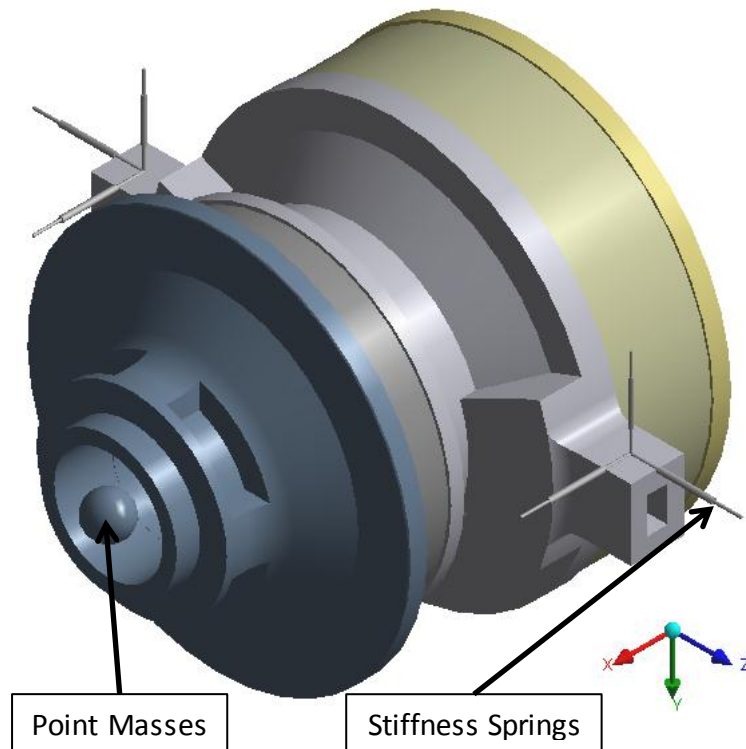
Figure 3.13: Simplified CGDT Housing with Boundary Conditions

This model is missing a rather large component, the generator. It has been ignored up to this point, because it is not the focus of this study. However, in order to accurately perform the analysis, the weight of the generator that is attached to the aft case of the CGDT housing could not be ignored. The added weight will play a role in altering the natural frequencies of the housing. Instead of adding an actual model, which would have made the meshing even more difficult, two point masses were added

to the center of the aft case. These two point masses represented the two components of the generator. This is assumed to be an appropriate substitution for the generator because both components are nearly symmetrical and have their center of gravity directly in the middle (at the end of the aft case). These point masses would provide a good approximation for the model. The two point masses had the values of $2,500\ kg$ and $5,250\ kg$ which matches the masses of the two main generator components.

It may be beneficial to remember that, as stated in Section 3.1, the internal components are ignored in this modal analysis in order to analyze the gearbox housing alone. Now that the model (Fig. 3.13) is complete with the boundary conditions added, the modal analysis can begin.

3.3.2: Modal Frequencies of the Gearbox Housing

ANSYS was used to perform modal analysis over the range of 0-1,000 Hz in order to ascertain the natural frequencies of the housing. This range was chosen to correspond to the range that is displayed within the waterfall plots from Chapter 2. The Table 3.2 displays the modal frequencies as obtained via ANSYS.

Table 3.2: Modal Frequency Results from ANSYS

Mode	Frequency (Hz)	Mode	Frequency (Hz)
1	1.7024	23	545.96
2	1.7686	24	560.16
3	3.5309	25	571.47
4	5.3358	26	611.76
5	32.082	27	617.82
6	51.294	28	642.59
7	180.24	29	658
8	188.61	30	664
9	234.29	31	674.9
10	280.16	32	681.86
11	286.79	33	701.45
12	308	34	702.55
13	308.22	35	714.66
14	361.83	36	728.81
15	386.65	37	729.4
16	395.27	38	766.25
17	431.61	39	767.32
18	437.57	40	790.78
19	459.46	41	815.82
20	485.52	42	817.13
21	529.05	43	833.37
22	530.56	44	872.4

3.3.2: Comparison to Experimental Data

The results from Table 3.2 are compared to the experimental trouble frequencies listed earlier in Table 2.3. There were several conclusions that were drawn from the ANSYS modal analysis. First, ANSYS did not predict modal frequencies that correlated to the excited frequencies that were seen in the experimental data.

Table 3.3: Experimental Data Comparison

Matching Frequencies	
Test Frequency (Hz)	ANSYS Match
8	NO
15	NO
20	NO
27	NO

The second important point can be deduced by closely inspecting all of the ANSYS modal analysis results shown in Table 3.2. It can be clearly seen that the predicted modal frequencies are very closely spaced and span the entire range. This makes any future structural modifications to avoid noise propagation a very difficult task.

3.4: Re-evaluation

The modal frequencies obtained in ANSYS reveal that the model does not predict the actual experiment. This leads us to believe that this system's dynamics is far more

complex than we had originally assumed. The previous assumption, that the internal components have a negligible interaction with the housing was called into question. Investigation into the literature of how previous researchers handled this modeling problem was conducted. According to Henriksson's [12] in depth study of gearbox noise, any accurate model of the gear system must include the gear mesh interactions. Henriksson's research, along with research by Åkerblom [15], show that there is a correlation between the transmission error (TE) and the resulting noise level. These studies support the idea that the interactions of the gears with the housing are of the utmost importance and play a large role in defining the resonances seen in the housing. Therefore, this short-cut approach of neglecting the influence of the internal components is inaccurate. For this reason, Chapter 4 attempts to establish a more complete picture by having a model that includes the entire test stand. By doing this, our hope is to account for all the interactions that play a role in defining the housing resonances.

CHAPTER 4: FREQUENCY RESPONSE ANALYSIS USING MASTA

A more comprehensive analysis approach using MASTA, a design and analysis software specifically for systems involving gears, is presented. A model of the entire test stand is presented and modified. The model's boundary conditions, and the assumptions behind them, are discussed. The results of the predicted orders, excitation frequencies, and mode shapes of the gearbox are shown. These are then compared to experimental data showing a strong correlation for both the orders and excitation frequencies and inconclusive comparison of the mode shapes.

4.1: Overview

The housing modal analysis performed in Chapter 3 with ANSYS did not produce results that matched the experimental data. Moving forward, a new approach will be used to account for the interactions between the internal components and the housing. To achieve this goal, a more complete computational model which includes all components must be created.

In this new approach, all of the forces produced by the gear meshes must be accounted for. To do this within ANSYS, tedious gear teeth force calculations would be needed. These forces would then have to be manually input into a force matrix and applied to the model. This can be a very time consuming and computationally demanding task. Instead of using ANSYS, a new software, MASTA, will be used to perform analysis. MASTA is a comprehensive computational environment used for the design, simulation and analysis of transmission systems. The gear meshes, and the forces created by them, are both incorporated into the noise, vibration, and harshness (NVH) analysis within MASTA. This is more than simply a modal analysis, it is a complete frequency response analysis. Therefore, more accurate results are expected with MASTA. At this point we have to start back over at the beginning of the Project Path laid out in Figure 3.1. The first step is to create a new model.

4.2: The MASTA Model

A far more complete and complex model of the test stand is created. Box 2 from Fig. 3.1 refers to the choice of the components to be included within the model. Instead of simply containing the five components of the housing, this model will be far more complex. Not only is the CGDT housing included, but all of the internal gears, bearings, and shafts are included as well. Referencing back to Fig. 2.2, the test stand contains the generator, a slave gearbox, and a driving motor. In order to more accurately capture the complex interactions that these components have on the resonances of the CGDT gearbox, many of these components are added to the model. Figure 4.1 shows the final model used within MASTA.
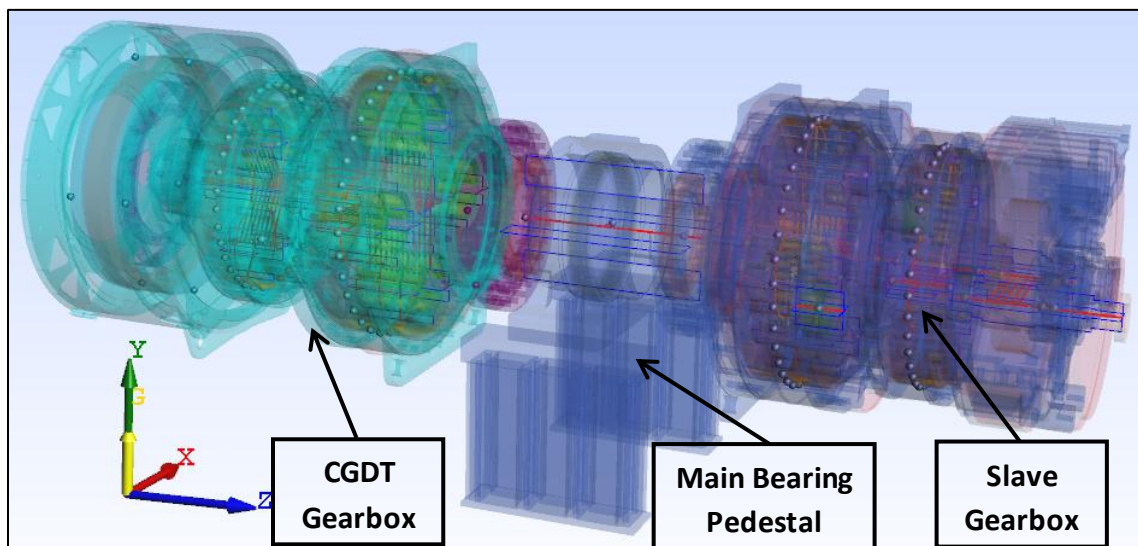
Figure 4.1: Isometric View of Transparent Test Stand Model in MASTA

The slave gearbox contains all of its internal gears, bearings, and shafts as well. The two gearboxes are connected to one another by the main shaft. This main shaft is supported by the main bearing pedestal. The generator is included on the back of the aft case of the CGDT gearbox. The one main component that is left out of this model is the driving motor. It is far removed from the CGDT and is bolted firmly to the floor. It is assumed that it has a negligible influence on the CGDT housing dynamics.

Box 2 from the Project Path in Fig 3.1 represents the simplification of the components within the model. The model was kept rather detailed with no simplification being made to the housing components, shafts, gears, bearings, or pedestals.

This model, as was said previously, does contain internal components. All of these components are added to the model and are represented by Box 3 from Fig. 3.1. The micro-geometry of each gear was input into the model. This allows for gear meshes to be accounted for in the analysis. The micro-geometery of the gears is confidential information that cannot be presented within this thesis.

4.3: Model Set Up

This portion of the thesis will lay out how MASTA is used to analyze the CGDT model. It will detail how the model is prepared for the analysis, as previously indicated within Box 5 of the Project Path, Fig. 3.1.

4.3.1: Boundary Conditions and Assumptions

The proper BC's are applied to this model. All of the interfacial surfaces between components were fixed. This is justified by the large number of bolts that hold the components together. The bottom surface of the main bearing pedestal was also fixed. This is to represent that it is firmly bolted to the ground. It is assumed that there are no significant motions at these points.

To account for the elastomeric mounts on which the torque arms (TAs) are mounted, a BC is applied. For this model, which includes the CGDT and the slave gearbox, there are four TAs that need to be accounted for. The appropriate stiffnesses and damping coefficients applied to represent these elastomers in Table 4.1.

Table 4.1: Elastomeric Material Dampening and Stiffness

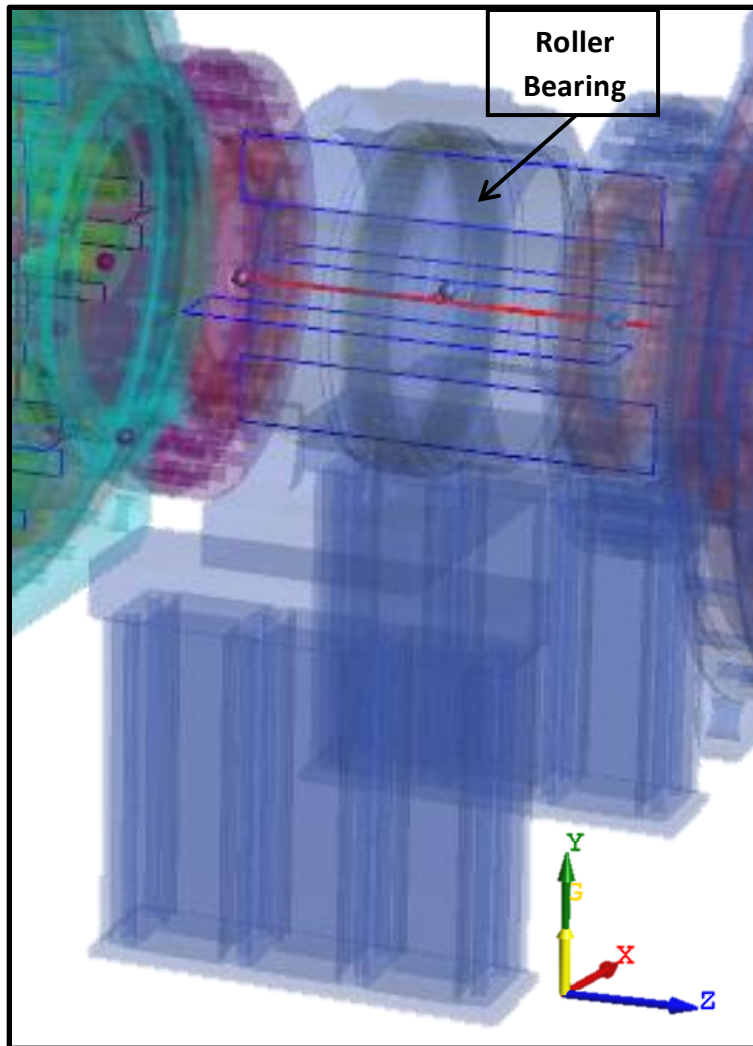| Elastomeric Material			
Dampening Value N/m	Stiffness Value kg/sec	ANSYS Model Axis	Test Stand Direction
1×10^6	1×10^6	X-axis	Horizontal
2×10^8	2×10^8	Y-axis	Vertical
1×10^6	1×10^6	Z-axis	Axial

Figure 4.2: Main Shaft Pedestal Bearing

The main shaft pedestal, shown in Figure 4.2, contains a roller bearing. This bearing aids in the alignment of the main shaft and dampens its movement. Therefore, this bearing is represented as a radial bearing load, and is assumed to have a strictly dampening influence which restricts motion of the main shaft to prevent misalignment. This BC is

dependent upon the material and design of the bearing itself. This information was used within the model but is confidential, and therefore can not be provided in this thesis.

4.3.2: Node Placement

Figure 4.3 shows the critical nodes, represented by the small spheres, where the frequency response analysis will be obtained. To acquire a holistic analysis, many nodes had to be used in order to accurately capture the mode shapes of the structure. To match the experimental data results from Chapter 2, nodes were also placed in the same locations as the accelerometers on the test stand. Based on their location, there were five nodes that were chosen to be analyzed in depth. These are listed in Table 4.2 with the corresponding sensor numbers and their locations on the test stand.

Table 4.2: Sensor Location Description

Sensor	MASTA Node	Test Stand Sensor	Sensor Location
1	1000001**8**	65001	Front Case: At 12 o'clock on the outside housing
2	1000000**7**	66001	Torque Arm: right TA when looking down wind
3	1000000**8**	66002	Torque Arm: left TA when looking down wind
4	1000005**4**	68002	Aft Case: near 11 olcock on the outside housing
5	1000000**5**	68001	Aft Case: surface between the upper and lower right pockets, as viewed from down wind
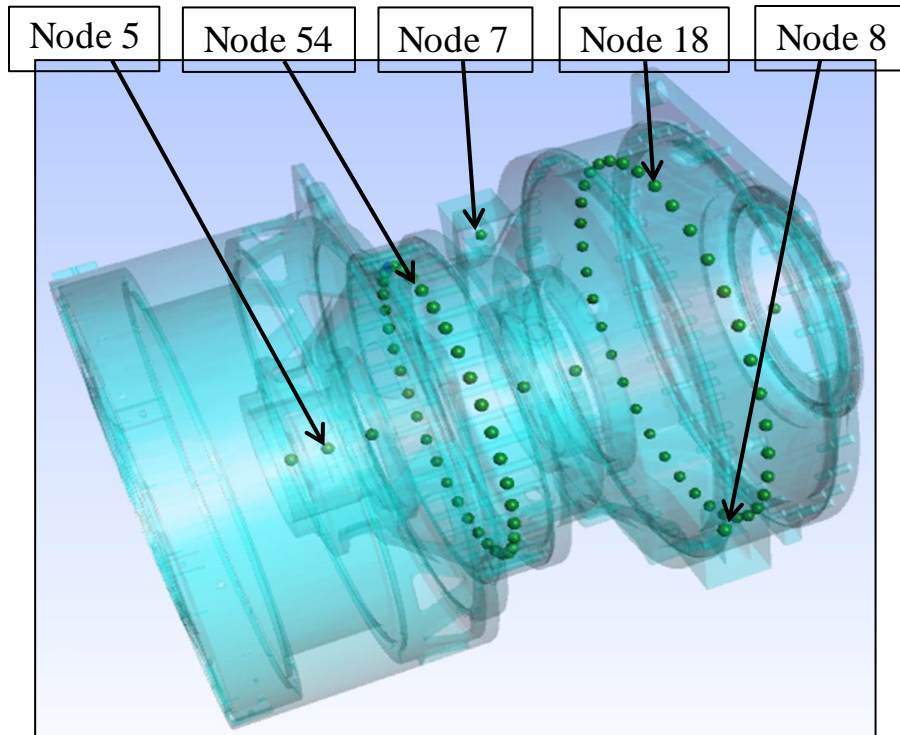
Figure 4.3: CGDT Housing with Node Locations Identified

4.4: Frequency Response Analysis

The process of running the analysis on the model within MASTA is described in this section, following Box 6 of the Project Path, Fig. 3.1. The Gear Whine Analysis within MASTA generates waterfall plots for each of the nodes within the model in all three directions. Within MASTA, the y-axis is interchangeable between displacement and acceleration. This allows both displacement and acceleration waterfall plots to be produced. Examples of the waterfall plots generated by MASTA, is shown in Figs. 4.4 and 4.5.
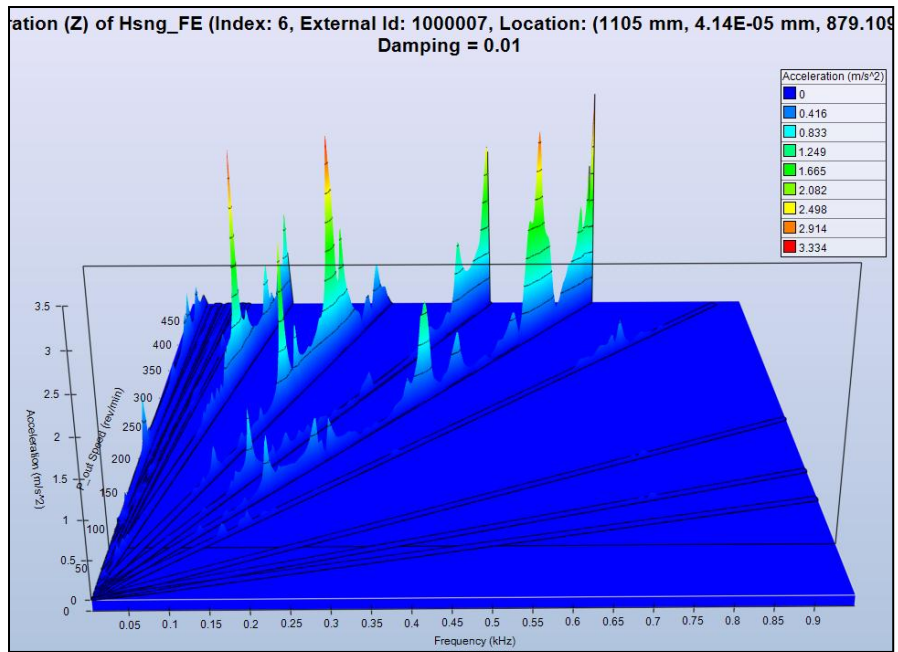
Figure 4.4: MASTA Produced Acceleration Waterfall Plot
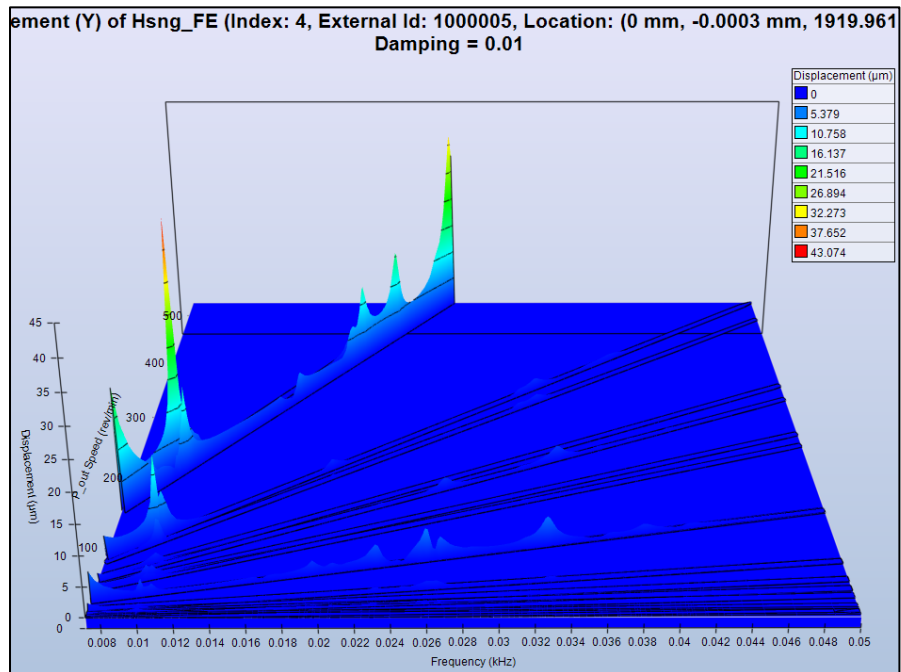
Figure 4.5: MASTA Produced Displacement Waterfall Plot

These waterfall plots are beneficial only if they match the waterfall plots obtained experimentally as presented in Chapter 2. Within MASTA, the plots can be adjusted in several ways. The P_out Speed (the generator rpm) is placed as the z-axis of the waterfall plots to correlate to the generator rpm used in the experimental data waterfall plots from Chapter 2. The x-axis is interchangeable between frequency and order. This allows, not only waterfall plots to be produced, but order plots as well. An example order plot is shown in Fig. 4.6.
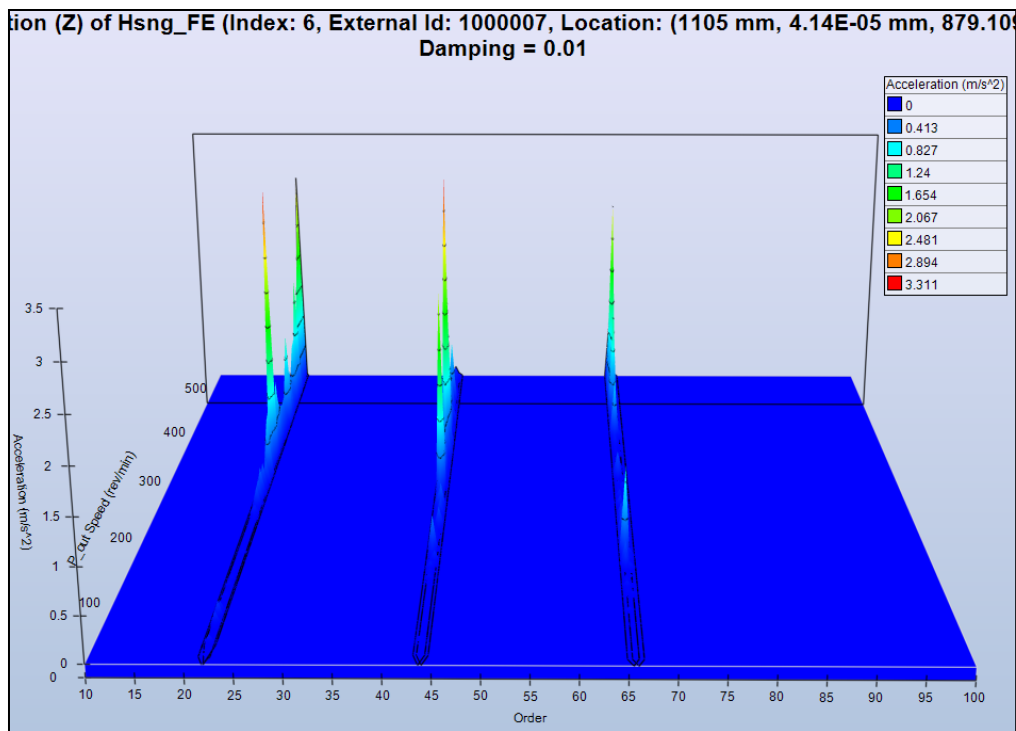
Figure 4.6: MASTA Produced Order Plot

These order plots are very similar to the waterfall plots created earlier in Chapter 2 and 4. The only difference is that instead of the amplitude being shown in terms of frequency, it is depicted in terms of the order itself. MASTA merely transforms the frequency values into order values by using Equation (2.1). Creating order plots makes the order lines easier to observe.

For the waterfall plots, the range for the x-axis can be adjusted manually. This, along with the other features, permits generating plots over the same range and with respect to the same characteristics as the experimentally collected data from Chapter 2. There is another aspect of MASTA's analysis that will be used to our advantage as well. This is represented by a 3-D model view that shows the shape of each vibration mode.

4.5: Results and Comparison

With the model set up as desired, the analysis begins. This section will present those results, and compare them to experimental data.

4.5.1: Order Comparison

As discussed in section 4.4, the graphical results are in the form of either order plots or waterfall plots. Either of these plots can be generated in terms of either displacement or acceleration. Figure 4.7 depicts an order plot with the order lines clearly identified.
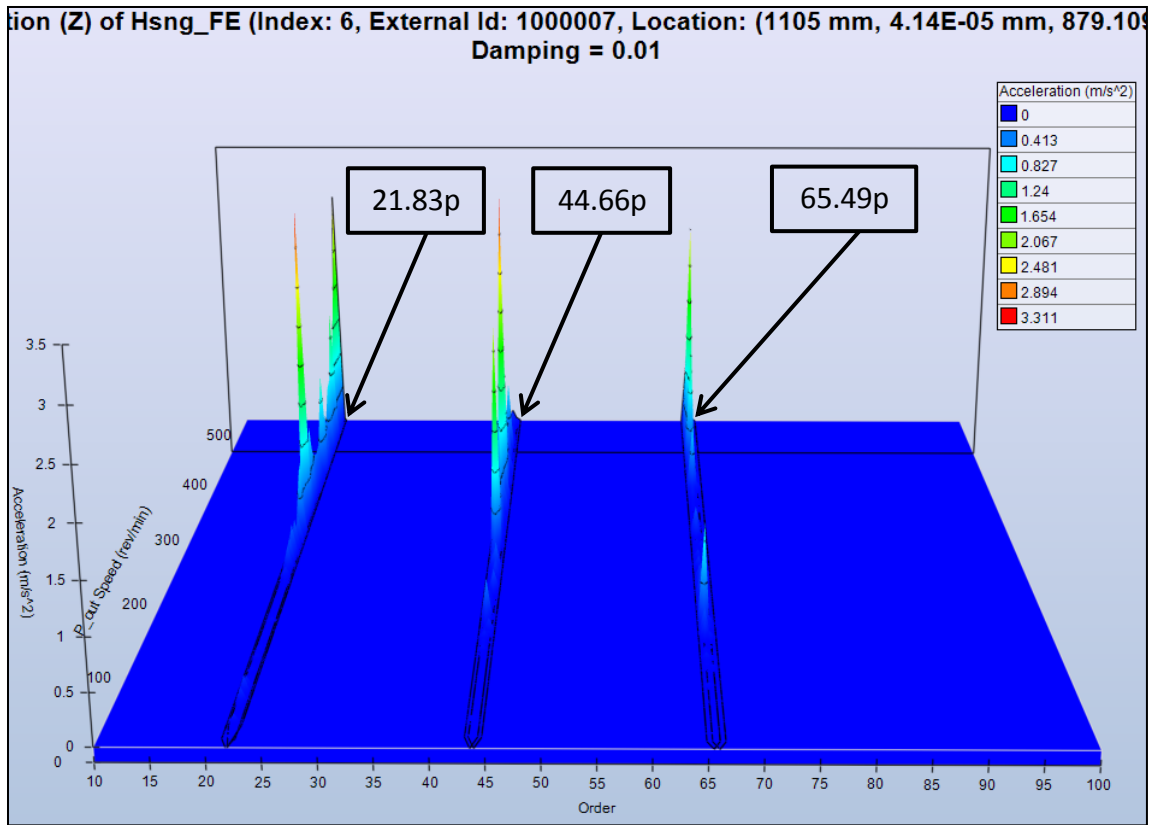
Figure 4.7: MASTA Produced Order Plot for Node 7

This plot provides the order lines and the corresponding amplitude response peaks present across a specified range of the generator rpm. Once all of the nodes of interest (Reference Table 4.2) were analyzed, the predicted orders were gathered. Although MASTA produces an unlimited amount of orders, only the significant orders, i.e. the orders that had relatively large spikes, were collected. In Fig. 4.7, the orders of 21.83p, 44.66p, and 65.49p are clearly present. By analyzing both the high frequency (acceleration waterfall plots) and the low frequency (displacement waterfall plots), for all of the nodes of interest, there were five orders in total that were found to be

significant. These are presented in Table 4.3 along with the experimentally observed orders shown in Table 2.2. Clearly, there is a very strong correlation between the two.

Table 4.3: Orders Comparison

Orders		
#	TEST STAND	MASTA ANALYSIS
1st	3.2	3.18
2nd	21.7	21.83
3rd	43.6	43.66
4th	65.5	65.49
5th	87.2	87.32

The MASTA model almost perfectly predicts the orders that were captured by the test stand data. The matching of the orders merely means that the model being analyzed has the correct gear ratio inputs for the CGDT and the slave gearbox. Even though it was encouraging that there is a strong correlation between the predicted results and the experimental data at this level, it is not as significant in terms of the dynamic behavior of the model.

4.5.2: Frequency Comparison

The orders having matched up, it is now time to move onto the frequency comparison. This comparison should give us a better idea of how accurately the model is predicting the interaction of all the components of the test stand, and more precisely, the frequencies which the CGDT housing components experience. Figures 4.8 and 4.9 are a sample of just two of the waterfall plots produced by MASTA
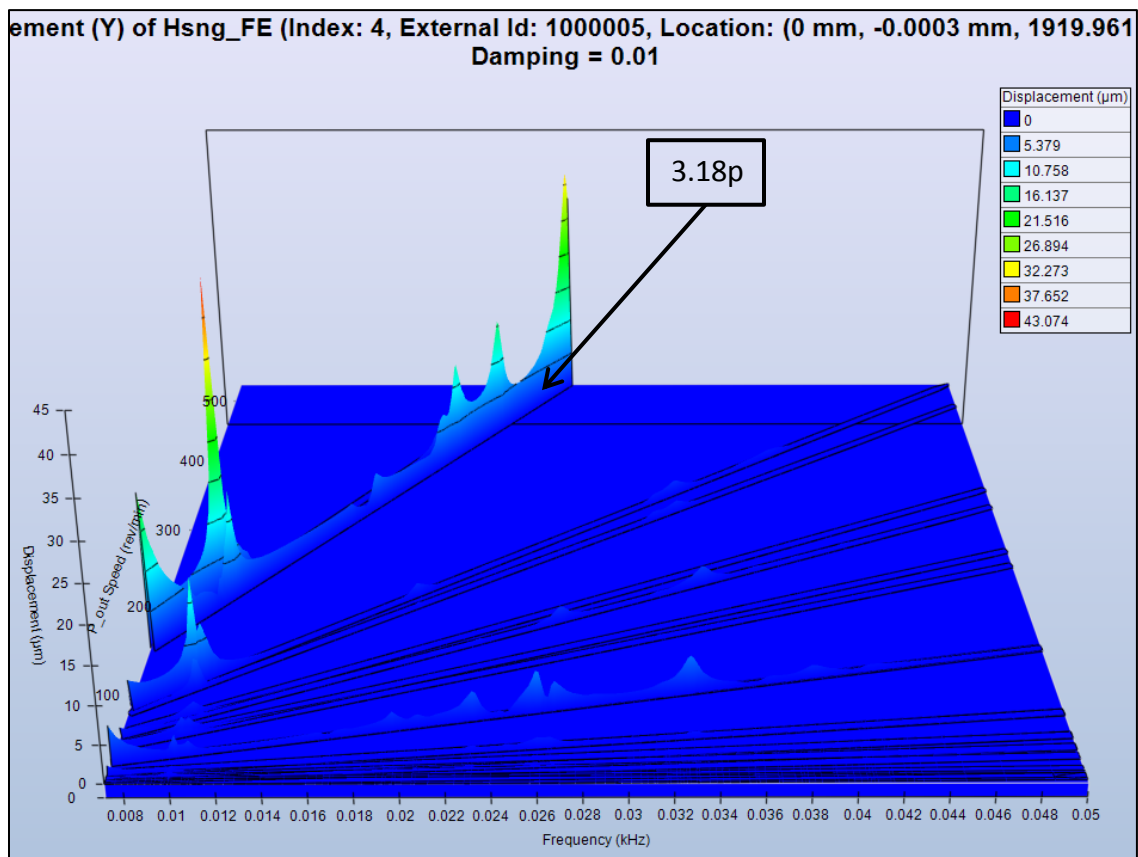
Figure 4.8: MASTA Produced Waterfall Plot for Vertical Displacement of Node 5

Figure 4.8 shows the amplitude response in terms of displacement. The frequencies along the x-axis cover the range from 0.001 to 50 Hz. All of this data is in terms of the generator speed (P_out Speed), which is shown in terms of rpm on the y-axis. The 3.18 order is also noted on this plot.
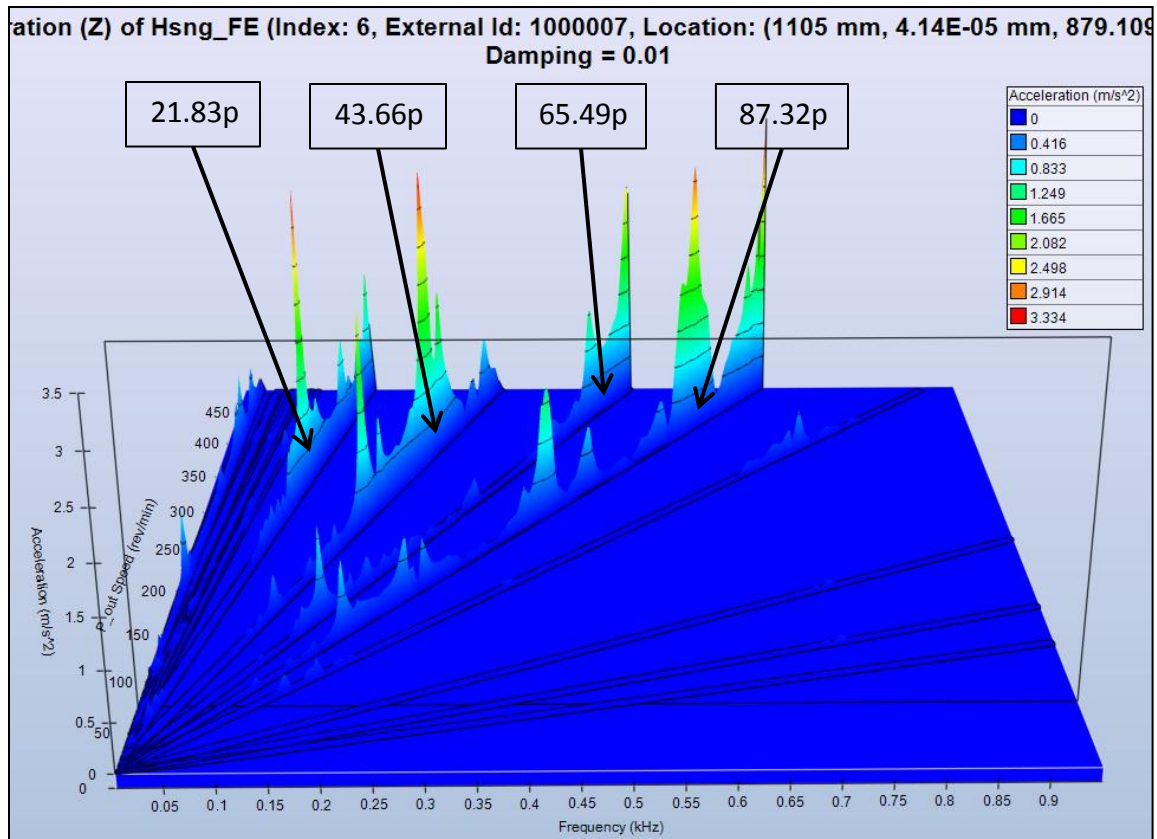
Figure 4.9: MASTA Produced Waterfall Plot for Axial Acceleration of Node 7

Figure 4.9 represents the same results but is in terms of acceleration and for a much wider range of frequencies. Here, four more order lines appear in the waterfall plot.

By observing the waterfall plots, it is seen that there are clear and definitive peaks within the response that actually lie on specific frequency lines and span more than one order. The frequencies at which these large responses occur, represent the problematic frequencies. It is these frequencies that will be compared to the experimentally collected data.
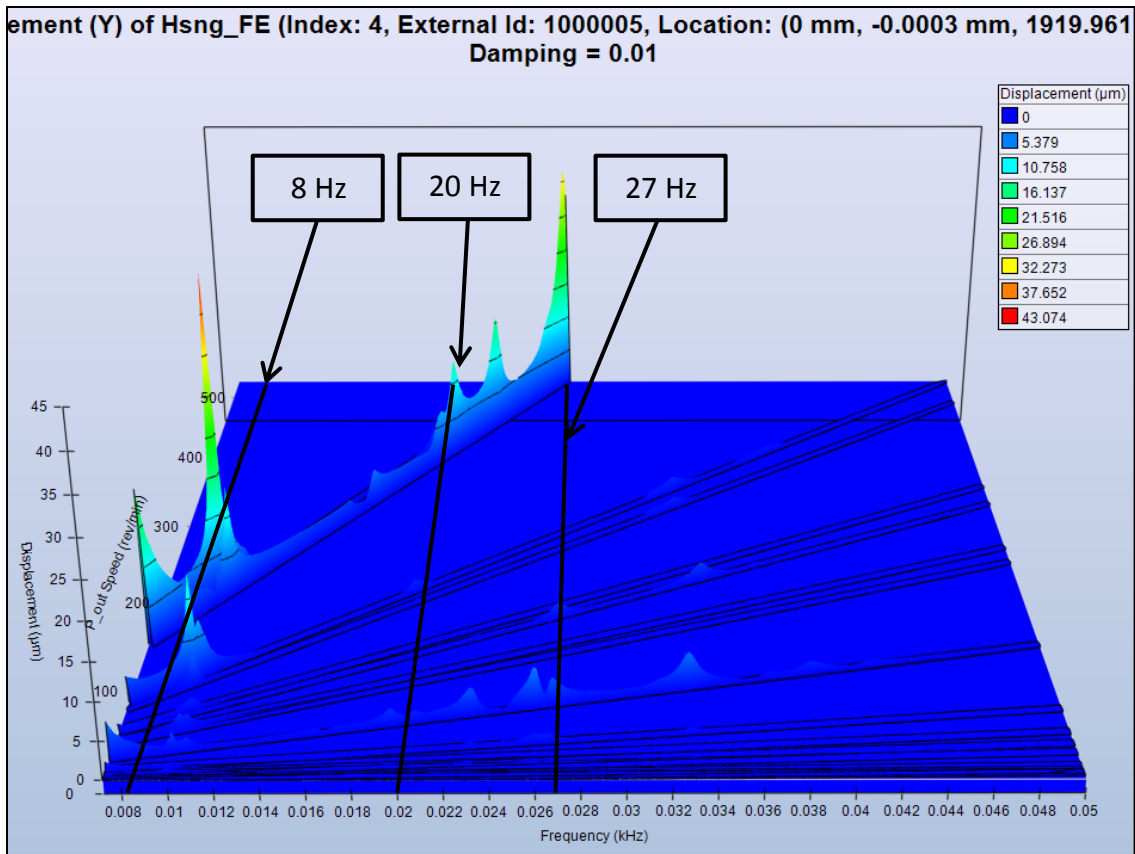
Figure 4.10: MASTA Produced Waterfall Plot with Frequencies Shown

Fig. 4.10 shows a particular displacement waterfall plot which contains two large peaks. These peaks occur at 8Hz and 27Hz which are depicted by the vertical frequency lines. The 20Hz line is drawn as well. Even though this is a smaller peak, it is still clearly evident within this displacement waterfall plot.

In the same manner, all of the displacement waterfall plots for all of the nodes from the MASTA analysis were examined. From the compilation of these results, and the test stand data results from Chapter 2, Table 4.4 is created. It provides the significant

excitation frequency values as observed in the test stand data. It then tells whether or not the model predicted the presence of those excitation frequencies and also gives the primary direction of the movement seen at those frequencies.

Table 4.4: Displacement Sensors Frequency Comparison

Frequencies		
Test Frequency [Hz]	Model Prediction	Primary Direction
8	YES	Axial, Vertical, and Horizontal
15	SOME	Vertical and Horizontal
20	YES	Axial, Vertical, and Horizontal
27	YES	No Correlation

All four excitation frequencies were predicted, however, only three of them had a strong correlation. The 15Hz frequency was present within the MASTA generated waterfall plots; however, it was not strongly present in the experimental data. The Primary Direction was determined by recording which test stand sensor picked up the excitation frequency and then comparing that direction to the direction shown in the 3D animation of the model in MASTA at that particular frequency. This indicates the primary direction that a particular node experiences while excited at a certain frequency. For the 8Hz, 15Hz, and 20Hz, the MASTA model had the same primary directions as the test stand. However, for the 27Hz, there was no correlation between the two.

The comparison results obtained using the acceleration sensors were much harder to infer. As described in section 2.3.3, no definitive peaks were shown within this data. Therefore, the only results that could be drawn from this comparison are based solely on common or uncommon trends between the model and the test stand. In the test stand, Fig. 2.4 the 21.7p and the 43.6p are definitely the dominant orders while the 65.5p and the 87.2p are significantly smaller for most of the sensors. Within MASTA, Fig. 4.4, all four of the orders are pretty similar in size. Also in the test stand, Fig. 2.4, there appears to be a continual ramp up in the order lines without ever hitting a peak within the range of 0-510rpm. This holds true for nearly all of the sensors. Within MASTA, Fig. 4.4, there is an overall increase in the response amplitude. However, there are peaks along the way. This makes it less of a continual increase as is seen in the experimental data of Fig. 2.4. Regardless of these peaks, the general trend of ever increasing magnitudes is present in both the test stand and the MASTA model.

In summary, there are some common trends between the model and the test stand data for the acceleration sensors. However, no concrete comparisons of exact excitation frequencies could be made. Overall, the model was shown to be mostly accurate in containing the excitation frequencies detected by the displacement sensors.

4.5.3: Mode Shapes Comparison

The last part of the comparison process is to determine how the mode shapes match up. To achieve this goal the 3-D animated model shapes produced by MASTA are

compiled. These mode shapes are then compared to verify that the model accurately predicts the physical response of the CGDT within the test stand. Based on data from the laser channels, and the 3-D mode shapes predicted by MASTA, Table 4.5 was created.

Table 4.5: Mode Shape Comparison

Mode Shapes	
Test Stand Obtained	MASTA Predicted
2 Hz	YES – 1.3, 1.5 Hz
9.7 Hz	Insufficient Data
18.4 Hz	Insufficient Data
20.5 Hz	Insufficient Data
23.4 Hz	Insufficient Data
27.3 Hz	Insufficient Data
40.8 Hz	Insufficient Data

Table 4.5 shows the mode shapes that were collected from the laser channels and tells whether MASTA predicted that mode shapes or not. MASTA predicted only one out of the seven modes shapes. At this point it is beneficial to look back at Table 2.5 and notice that the only rigid body mode predicted by the laser channels is the first one, and that this mode is predicted by MASTA. It is believed that the four laser channels are insufficient for predicting the non-rigid body mode shapes. To obtain a more complete picture a larger number of laser channels would be needed. The insufficient data from only four laser channels is believed to be the reason why the MASTA predicted mode shapes did not match the laser channel mode shapes that were non-rigid.

The one mode shape that was accurately captured by MASTA and this is the rigid body rotation of the system about the main bearing (reference Table 2.5 for mode shape description) as depicted in Fig. 4.11.
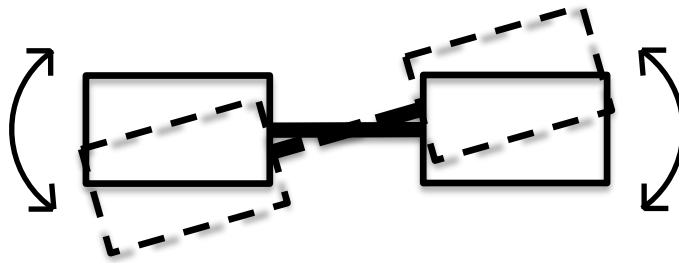
Figure 4.11: Diagram of Observed Mode Shape at 2Hz

Figure 4.11 is an overhead view of a simple diagram of the test stand showing the two gearboxes connected by the main shaft. The solid lines depict the original position, and the dashed lines represent the transformed position. The arrows are added to indicate the direction of motion. This motion was predicted by MASTA at two separate frequencies, 1.3Hz and 1.5Hz.
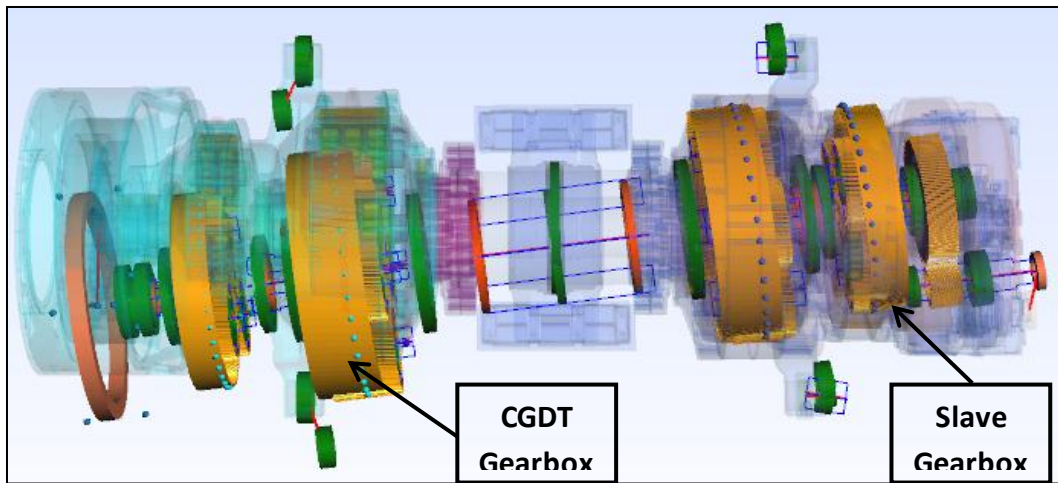
Figure 4.12: Screenshot of MASTA Mode Shape at 1.3Hz
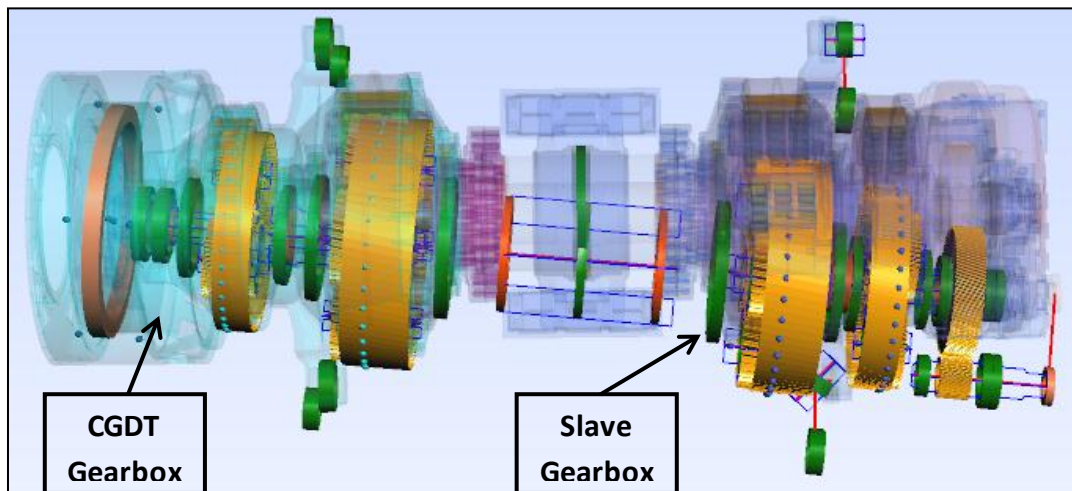
Figure 4.13: Screenshot of MASTA Mode Shape at 1.5Hz

These are simply screenshots of the top view of the model, so the motion can not be observed. Both of these mode shapes contain motion similar to what is shown by the arrows in Fig. 4.11. MASTA predicted two very similar mode shapes at just slightly different frequencies. Notice that for the mode shape associated with 1.3Hz frequency,

the CGDT has a larger motion, while the 1.5Hz the Slave Gearbox has the larger motion. The reason behind the presence of these two similar closely-spaced modes in MASTA stems from the fact that the CGDT Gearbox has a slightly larger mass due to the mass of the attached generator. Experimentally, however, since the modes are so closely spaced the laser channel was able to predict only one peak

Overall, when comparing the mode shapes to confirm the MASTA model there is not a strong correlation. Though MASTA did predict the rigid body rotation mode shape very close to 2Hz, it was determined that only four laser channels to collect displacement data was insufficient to capture the complete picture of non-rigid body movement.

CHAPTER 5: CONCLUSIONS AND FUTURE WORK

This portion of the thesis will briefly recount what has been accomplished within this project and the conclusions that came about as a result. Several comments will be made as to how this research, and the results obtained through it, will help future work in this area, specifically within GE.

5.1: Housing Modal Analysis Conclusions

ANSYS was used within the first part of this project. Although it did not turn out to be a very useful tool to use for this problem, it still did provide several important characteristics of the CGDT gearbox. In particular, ANSYS demonstrated that many of the assumptions used in creating the model were in fact critical, contributing components to the dynamic behavior of the CGDT housing. In summary, it was assumed that any interactions that the internal components, or even the drive shaft, have on the CGDT housing were negligible. However, it was discovered through comparison with experimental data that this is not an accurate assumption. It turns out that gear meshes are vitally important in determining the behavior of the housing. As such, the entire test stand rig had to be modeled to incorporate all of the interactions that exist within the system.

5.2: Frequency Response Conclusions

Although the final conclusion of the MASTA analysis came up short in some aspects, there was an immense amount of progress made using this model. It is clear by comparing the MASTA model, which includes internal components and the entire test stand rig, to the ANSYS model, and the results that came from the different analysis, that the housing dynamics is affected by the internal components. The MASTA model accurately captured all of the order and most of the excitation frequencies that were

present within the experimental data. The rigid body mode shapes were accurately predicted but there was insufficient data from the laser channels to obtain the non-rigid body movement. This type of detailed analysis on a gearbox was a great breakthrough for GE.

5.3: Future Recommendations

Having developed a basis model to work from, future work in this area should be concentrated on enhancing the model's accuracy. It is believed that the most important aspects to consider in creating a more detailed model is to better specify the boundary conditions and to include the effect that all of the other components. Based on this, future studies should be devoted to the influence that the gearbox design has on the excitation frequencies. This will allow a simple model redesign and a quick analysis to be performed, so as to determine whether or not the new design shifts the excitation frequencies away from the natural frequencies present within the housing components.

This research was unique in the fact that when it began, all of the test stand data had already been collected. Throughout this project it was seen time and time again how difficult it is to use data that was collected and then attempt to compare it to the predicted dynamic behavior of the CGDT gearbox. Now that a process for modeling, and subsequently analyzing, a gearbox has been determined, the way in which this analysis works can help for any future work. The next time that tests are run with the test stand,

the sensors and their locations can be more strategically chosen knowing how MASTA's analysis will run. Specifically with respect to the laser channels to determine the mode shapes. It was seen that only four laser channels were used to predict the mode shapes of the complex test stand which was insufficient for predicting any non-rigid body mode shape. The number of laser channels should be increased in order to obtain a more complete representation of the response of the test stand.

An argument was made, based on the ANSYS modal analysis, that the large number of the closely-spaced frequencies present in the system's dynamics will render a design that satisfies the trouble frequencies inefficient. Because of this, it is encouraged that GE investigate more into tuned vibration absorbers to dampen the amplitude response at a specific frequency. These systems could then be tuned to have a natural frequency equal to one of the trouble frequencies within the gearbox. The energy of this one frequency would then be absorbed and dissipated as heat or electricity. This concept has been applied with great success in absorbing and dissipating vibrations in other applications. The concept of adding a spring-mass-damper system into the design of the gearbox, may be extremely beneficial. Also, instead of merely examining passive controls, active methods of vibration control should be explored as well. The tuned spring-mass-damper system only absorbs a single frequency. Active mass dampers are able to absorb more than just a single frequency because they are actively controlled in order to alter their stiffness. When the stiffness is varied, the natural frequency of the damper will vary proportionally. One of the most common controllers for such systems

is based on using active materials. In order to absorb and dissipate all of the trouble frequencies with one system, this active mass damper could be extremely advantageous.

The groundwork has been laid for creating a model that is valuable to several different groups within GE. For starters the Tonality Team investigates similar topics to those that were covered in this research, and therefore, can use this information, and more importantly this process, to allow them to use MASTA as a tool for solving some of the issues that they face. This includes the drivetrain but can encompass other components of a wind turbine. Most importantly, the process of analyzing the CGDT here in this thesis can be extremely beneficial to future gearbox designs. Now, new designs can have preliminary analysis run within MASTA before any prototyping and full-scale testing is carried out. This will hopefully save a lot of time and large amounts of money for GE. It will, more importantly, improve their design process so that it is easier and quicker to design the world's best wind turbines.

References

[1]   Mathew, Sathyajith. *Wind Energy: Fundamentals, Resource Analysis, and Economics*. Berlin: Springer, 2006. Print.

[2]   Musgrove, Peter. *Wind Power*. Cambridge: Cambridge UP, 2010. Print.

[3]   Righter, Robert W. *Windfall: Wind Energy in America Today*. Norman: University of Oklahoma, 2011. Print.

[4]   Tong, Wei. *Wind Power Generation and Wind Turbine Design*. Southampton: WIT, 2010. Print.

[5]   "The Reality of U. S. Energy Incentives." *Awea.org*. American Wind Energy Association, 2011. Web. Dec. 2013.

[6]   "Renewable Energy Sources in the United States." *Nationalatlas.gov*. National Atlas of the United States of America, 14 Jan. 2013. Web. Jan. 2013.

[7]   "IEA Wind Annual Report 2011." *ieawind.org*. International Energy Agency Wind, Jul. 2012. Web. Dec. 2012.

[8]   Bolinger, Mark, and Ryan Wiser. "2011 Wind Technologies Market Report." *Energy Efficiency and Renewable Energy*. U.S. Department of Energy, Aug. 2012. Web. Dec. 2012.

[9]   The European Wind Energy Association. *Wind Energy: The Facts.* EWEA, n. d. Web. Nov. 2012.

[10]   "noise." *Merriam-Webster.com*. 2013. http://www.merriam-webster.com (28 Feb. 2013).

[11]   Rogers, Anthony L., James F. Manwell, and Sally Wright. "Wind Turbine Acoustic Noise." Renewable Energy Research Laboratory, Jan. 2006. Web. Aug. 2012.

[12]   Henriksson, Mats. *On Noise Generation and Dynamic Transmission Error of Gears*. Thesis. Royal Institute of Technology School of Engineering Sciences, 2009. Stockholm: KTH, 2009. Print.

[13]   Smith, James D. *Gear Noise and Vibration*. New York: Marcel Dekker, 2003. Print.

[14]   Platten, Michael F. "Measuring Gear Transmission Error inside a Loaded, Running Gearbox Is the Perfect Tool for Detecting and Diagnosing Gear Noise. Romax Technology Explains." *GEAR Solutions* Jan. 2011: n. pag. Web. 25 Mar. 2013. <http://www.gearsolutions.com/article/detail/6051/troubleshooting-gear-noise>.

[15]   Åkerblom, M., 2008, *Gearbox Noise, Correlation with Transmission Error and Influence of Gearing Preload,* Ph.D. thesis, Department of Machine Design, Royal Institute of Technology, tRITA-MMK 2008:19, ISSN 1400-1179

[16]   Yildirim, N., G Gasparini, and S Sartori. "An improvement on helicopter transmission performance through use of high contact ratio spur gears with suitable profile modification design," Proc. IMechE Part G: *Journal of Aerospace Enginering*, 222.8 (2008): 1193-1210. Web. Dec. 2012

[17]   Houser, D. R., Oswald, F. B., Valco, M. J., Drago, R. J., and Lenski, J., 1994, "Comparison of transmission error predicitons with noise measurements for several spur and helical gears," 30th *AIAA/ASME/SAE/ASEE joint propulsion conference,* Indianapolis.

[18]   Hjort, S, et al. "Prediction and Reduction of Noise from a 2.3 MW Wind Turbine." *Journal of Physics: Conference Series* 75 (2007): Web. Dec. 2012.

[19]   "Monthly Electricity Statistics November 2012." *Iea.org*. International Energy Agency, 2013. Web. Jan. 2013.

[20]   "A Summary of Opinions Surveys on Wind Power." *Ewea.org*. The European Wind Energy Association, n.d. Web. Aug. 2012.

[21]   "Statistics on China's Wind Development." *gwec.net*. Global Wind Energy Council, n.d. Web. Nov. 2012.

[22]   "Wind in Numbers." *gwec.net*. Global World Energy Council, n.d. Web. Nov. 2012.

[23]   Vandenberg, G. P. "Effects of the Wind Profile at Night on Wind Turbine Sound." *Journal of Sound and Vibration* 277.4-5 (2004): 955-70. Print.

[24]   Dinner, Hans. "Showing the Teeth at the Wind." *kisssoft.ch*. KISS Soft, n.d. Web. Nov. 2012.

[25]   Rosenbloom, Eric. "A Problem With Wind Power." *aweo.org*. N.p., Sept. 2006. Web. July 2012.